Phenomenology of k-essence dark energy in the Cosmic Microwave Background

Liao, Dehong

Phenomenology of k-essence dark energy in the Cosmic Microwave Background

THESIS

submitted in partial fulfillment of the
requirements for the degree of

MASTER OF SCIENCE
in
PHYSICS

Author :	Dehong Liao
Student ID :	Removed due to privacy reasons
Supervisor :	Dr. A. Silvestri
Second corrector :	Dr. S.P. Patil

Leiden, The Netherlands, August 1, 2024

Phenomenology of k-essence dark energy in the Cosmic Microwave Background

Dehong Liao

Huygens-Kamerlingh Onnes Laboratory, Leiden University
P.O. Box 9500, 2300 RA Leiden, The Netherlands

August 1, 2024

Abstract

K-essence dark energy is a generalization of quintessence dark energy by promoting the canonical kinetic term X to a function of X and the field ϕ. K-essence dark energy can serve as a kind of Early Dark Energy (EDE) which energy contribution to the universe is limited in a narrow redshift window around the time of recombination and then dilutes way. EDE is a potential solution to Hubble tension, which refer to the fact that the local measurements give a Hubble constant that is not consistent with the value inferred from early-universe data such as cosmic microwave background. In this paper, we proposed a ξX^2 EDE model which includes a non-canonical kinetic term ξX^2 as an attempt to resolve the Hubble tension and discuss its dynamics in detail. After performing Markov Chain Monte Carlo analyses, we find ξX^2 EDE model predicts a Hubble constant H_0 of $71.09^{+0.84}_{-0.72}$ km/s/Mpc using a collection of datasets and is in agreement with SH0ES determination $H_0 = 73.04 \pm 1.04$ at $\sim 1.5\sigma$. A model parameter ξV_i is 2 σ non-zero supporting the existence of ξX. The overall fit to the datasets in our model is improved by -21.2 compared with ΛCDM when analysing with a SH0ES' H_0 prior.

Contents

Chapter 1

Introduction

1.1 ΛCDM model

The ΛCDM model, or the Lambda cold dark matter model, is the current standard model of cosmology. It has proven to be simple, extremely predictive and robust against observation. In this section, we would like to provide a self-contained description, which help to understand the pillars of the model as well as why and how we will go beyond ΛCDM.

- Mathematical Foundation: General relativity

At large scales, gravity is the only relevant force that will influence the dynamics of the universe. General Relativity (GR) is a geometric theory of gravitation published by A. Einstein in 1915. In GR, gravity is a geometric property of the four-dimensional spacetime and the math used to describe it is differential geometry. The Einstein's field equations, which relates the geometry of spacetime with matter within it, can be written as:

$$R_{\mu\nu} - \frac{1}{2}Rg_{\mu\nu} + \Lambda g_{\mu\nu} = 8\pi G T_{\mu\nu} \tag{1.1}$$

where Greek letters μ, ν represents spacetime coordinates, $\mu, \nu = 0, 1, 2, 3$ (On contrary, Latin letters represents spatial coordinates, i,j, ... = 1,2,3). Hereinafter we use c = 1 unless otherwise stated. $R_{\mu\nu}$ is the Ricci tensor and R is the Ricci scalar, $R = R^{\mu}_{\mu}$, $g_{\mu\nu}$ is the metric tensor, $T_{\mu\nu}$ is the energy-momentum tensor and G is the Newton gravitational constant. Finally we note that Λ appears in the equations, which is the so-called cosmological constant (CC).

- Physical assumptions

The most important assumption made within ΛCDM is the so-called Cosmological Principle, stating that our universe is **isotropic** and **homogeneous** everywhere. Being isotropic at some points in the universe means space looks the same at these points in all direction, while homogeneity implies the metric is the same throughout the universe. Isotropy and homogeneity can well describe the observed nature of the universe.

In a isotropic, homogeneous and expanding universe, the metric has the following form:

$$ds^2 = g_{\mu\nu}dx^\mu dx^\nu = -dt^2 + a^2 d\sigma^2 \tag{1.2}$$

where

$$d\sigma^2 = \frac{dr^2}{1-kr^2} + r^2 d\Omega^2 \tag{1.3}$$

when writing metric, we are using the (-,+,+,+) convention. Here r is the comoving coordinate and a = a(t) is the scale factor. This metric is the Friedmann-Lemaître-Robertson-Walker (FLRW) metric when taking curvature k into account. k is often normalize to:

$$k \in \{-1, 0, 1\} \tag{1.4}$$

k = -1 corresponds to a constant negative curvature which describes a open universe. k = 1 corresponds to a constant positive curvature and close universe, while k = 0 corresponds to no curvature, i.e., flat universe.

Measurements shows that we are living in a **flat** universe, in this case the FLRW metric is given by:

$$ds^2 = -dt^2 + a^2(dx^2 + dy^2 + dz^2) \tag{1.5}$$

It is useful to introduce the conformal time η:

$$\eta(t) \equiv \int_0^t \frac{1}{a(t')} dt' \tag{1.6}$$

In terms of η, the FLRW metric in a flat spacetime can be written as:

$$ds^2 = a^2(-d\eta^2 + dx^2 + dy^2 + dz^2) \tag{1.7}$$

An important quantity we will be discussing throughout this work is the Hubble parameter describing the expansion rate of the universe:

$$H = \dot{a}(t)/a(t) \equiv \frac{da(t)}{dt}/a(t), or, \mathcal{H} = a'(\eta)/a(\eta) \equiv \frac{da(\eta)}{d\eta}/a(\eta) \tag{1.8}$$

and today's Hubble parameter $H(t_0)$ is denoted as H_0. H_0 has the unit km/s/Mpc, and sometimes we also use another dimensionless parameter h, $h = H_0/(100km/s/Mpc)$.

- Constituents of the Universe

In the above discussion, we denote all constituents (except for CC) of the universe, or the right hand side of Einstein field equations, as matter. From now on, we divide this general 'matter' into normal baryon matter, cold dark matter (CDM), photon and neutrino. The first two and the last two species are often called 'matter' and radiation, respectively.

In background cosmology, matter, radiation and cosmological constant are all considered as perfect fluids, which can be completely characterized by the rest-frame mass density ρ (also dubbed as energy density) and the isotropic rest-frame pressure p (or simply pressure). A minimally coupled scalar field can also be regarded as a perfect fluid. The general form of the energy-momentum tensor for a perfect fluid is:

$$T^{\mu\nu} = (\rho + p)U^{\mu}U^{\nu} + pg^{\mu\nu} \tag{1.9}$$

where $U^{\mu} = dx^{\mu}/dt$ is the four-velocity of the fluid with respect to the observer.

Under this construction, the energy density and pressure for a species i can be read from the energy momentum tensor:

$$\rho_i = -T^0_0 \tag{1.10}$$

$$p_i = \frac{1}{3}T^j_j \tag{1.11}$$

A equation of state (EoS) parameter is defined for the perfect fluid:

$$w = \frac{p}{\rho} \tag{1.12}$$

In cosmology, matter is pressureless, $w_m = 0$, radiation has $w_r = \frac{1}{3}$ while $w_\Lambda = -1$

- The Friedmann equations

Einstein's field equations are the fundamental equations for ΛCDM and essentially all results in cosmology can be derived from the them. In its most general form, Einstein's field equations is a set of ten partial differential equations. However, after adopting the FLRW metric, the number of independent equations can be reduced to two, which are the Friedmann equations:

$$H^2 = \frac{8\pi G\rho}{3} + \frac{\Lambda}{3} \tag{1.13}$$

(1st Friedmann equation), and

$$\frac{\ddot{a}}{a} = -\frac{4\pi G}{3}(\rho + 3p) + \frac{\Lambda}{3} \tag{1.14}$$

(2nd Friedmann equation)

Eq (1.13) is the 00 component of Eq (1.1), while Eq (1.14) is a linear superposition of Eq (1.13) and the ii component of Eq (1.1).

The continuity equation can also be derived:

$$\dot{\rho} + 3H(\rho + p) = 0 \tag{1.15}$$

When studying the dynamics of the universe, the dimensionless density parameter is useful:

$$\Omega_i = \frac{\rho_i}{\rho_{crit}} \tag{1.16}$$

where the critical density ρ_{crit} is the total energy density of a flat universe:

$$\rho_{crit} = \frac{3H_0^2}{8\pi G} \tag{1.17}$$

Then in ΛCDM we have:

$$\Omega_m + \Omega_r + \Omega_\Lambda = 1 \tag{1.18}$$

- Cosmological constant or dark energy

Cosmological constant is introduced (again, after A. Einstein abandoned it well-before the foundation of ΛCDM) to ΛCDM to explain the accelerated expansion of the universe [1]. The origin of cosmological is not stated in ΛCDM, but historically a possible explanation to it is related to the vacuum energy density ρ_V, which has a energy momentum tensor of the form:

$$< T_{\mu\nu} >_V = -\rho_V g_{\mu\nu} \tag{1.19}$$

compare it with Eq (1.1) assuming no matter or radiation exists, it is straightforward to find that $\rho_\Lambda = \rho_V$. However, very intuitively, the scale of the vacuum energy can be estimated by [2][3][4]:

$$\rho_V \sim \int_0^{M_{max}} \frac{4\pi k^2 dk}{(2\pi)^3} \frac{1}{2}\sqrt{k^2 + m^2} \sim M_{max}^4 \tag{1.20}$$

where M_{max} is the cutoff scale, m is the mass of the field that contributes to the vacuum energy. If the known particles in Standard Model are to make vacuum contribution, M_{max} should be about 100 GeV, leading to a $\rho_V \sim 10^8 GeV$. However, this is greater than the observed value of ρ_Λ by about 54 orders of magnitude. A possible solution to it is introducing another field that cancels ρ_V no matter how large it is. To do so, the energy density of this field should be extremely fine-tuned, causing the so-called fine-tuning problem.

To circumstance this worrisome problem, people proposed to interpret cosmological constant as a separate component of the Universe, namely the Dark Energy (DE). The simplest example of DE is *quintessence* [5][6], in which DE is a scalar field ϕ with action:

$$S = \int d^4x\sqrt{-g}(X - V(\phi)) \tag{1.21}$$

where $X \equiv -\frac{1}{2}g^{\mu\nu} \bigtriangledown_\mu \phi \bigtriangledown_\nu \phi$ is the canonical kinetic energy and $V(\phi)$ some potential.

Upon the assumption of FLRW metric, the energy density and pressure of the scalar field is:

$$\rho_\phi = \frac{1}{2}\dot{\phi}^2 + V(\phi) \tag{1.22}$$

$$p_\phi = \frac{1}{2}\dot{\phi}^2 - V(\phi) \tag{1.23}$$

Quintessence's EoS parameter is:

$$w_\phi = \frac{p_\phi}{\rho_\phi} = \frac{\frac{1}{2}\dot{\phi}^2 - V(\phi)}{\frac{1}{2}\dot{\phi}^2 + V(\phi)} \tag{1.24}$$

such that $w_\phi > -1$ and approximate CC (w = -1) when V is is completely flat.

Many DE models are not connected to canonical terms, for example, K-essence [7] and Galileon dark energy [8]. In **K-essence**, the Lagrangian is a function of X and ϕ, i.e., it has the action:

$$S = \int d^4x\sqrt{-g}K(\phi)\tilde{p}(X) \tag{1.25}$$

The introduction of non-canonical kinetic term has interesting consequences and we will show it in the rest of this work.

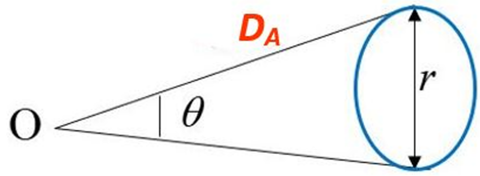

Figure 1.1: *Definition of angular diameter distance, source:[61]*

1.2 The Hubble tension

1.2.1 Tension between early and late time determination of H_0

The Hubble constant H_0 can be determined through a variety of methods. These methods can be can divided into local late-time measurements and the those depend on early-universe observation (e.g., CMB) assuming ΛCDM. These methods give mean values of H_0 varying from 67 km/s/Mpc to 76 km/s/Mpc [9], while the most severe tension appears between SH0ES' result 73.04 ± 1.04 [10] and PLANCK 2018's result 67.27 ± 0.54 [11], with the difference reaching $\sim 5\sigma$. We would like to briefly discuss the methods used by them.

- Inferring H_0 from CMB data assuming ΛCDM

Consider an object of comoving scale r in the universe, when observing from earth, it subtends an angle of θ, which is the angular size of the object, $D_A \equiv \frac{r}{\theta}$ is the comoving angular diameter distance. For an illustrative picture, see Fig. (1.1)

If we define the comoving sound horizon of last-scattering surface as $r_s^\star$, then we have:

$$\theta_s^\star = \frac{r_s^\star}{D_A^\star} \tag{1.26}$$

where $\theta_s^\star$ and $D_A^\star$ are the angular size angular size and comoving diameter distance of last-scattering surface, respectively.

$r_s^\star$ and $D_A^\star$ can be expressed as:

$$r_s^\star = \int_{z_\star}^{\infty} \frac{c_s(z')}{H(z')} dz' \tag{1.27}$$

$$D_A^\star = \int_0^{z_\star} \frac{1}{H(z')} dz' \tag{1.28}$$

where $c_s(z) \equiv (3(1+R(z)))^{-1/2}$ is the sound speed of the photon-baryon fluid, $R(z) \equiv \frac{3\rho_b}{4\rho_\gamma} = \frac{1}{z+1}\frac{3\omega_b}{4\omega_\gamma}$ is the baryon-to-photon energy ratio, $\omega_i = \Omega_i h^2$, i = baryon, cdm, radiation and Λ. [12][13]

Ignoring the cosmological constant, all terms on the right hand side of Eq (1.27) depends on ω_b, ω_r and ω_m. ω_r is precisely measure by CMB temperature, so $r_s^\star$ depends only on ω_b and ω_m. Briefly speaking, ω_m is determined through its impact on potential envelope, a scale-dependent boosting of oscillation power, which can be read from CMB power spectra. Variations of another quantity, ω_b, will change the peak heights in CMB temperature power spectra as well as the damping scale, thus can also be derived from CMB.

Finally, we note that $\theta_s^\star$ is related to the spacing between peaks in CMB spectra as $\theta_s^\star = \pi/\Delta\ell$. [14]. We combine Eq (1.26 - 1.28) to give:

$$\theta_s^\star = \frac{H_0 r_s^\star}{c\int_0^{z_\star}\frac{dz'}{E(z')}} \tag{1.29}$$

where E(z) is the dimensionless normalized Hubble parameter:

$$E(z) \equiv \frac{H(z)}{H_0} = \sqrt{\Omega_{m,0}(1+z)^3 + \Omega_{r,0}(1+z)^4 + 1 - \Omega_{m,0} - \Omega_{r,0}} \tag{1.30}$$

where $\Omega_{i,0}$ is today's value of Ω_i.

The denominator on the right hand side of Eq (1.29) is determined by local measurements. We can conclude that $H_0 r_s^\star = const$, so H_0 can be calculated using the information about CMB.

- Local Measurement: Luminosity distance of SNIa

When we measures the energy flux of a luminous source of absolute luminosity L at a distance d_L from earth, we are actually measuring its apparent luminosity l:

$$l = \frac{L}{4\pi d_L^2} \tag{1.31}$$

where d_L is called the luminosity distance. In an expanding flat universe, the luminosity distance can be written as:

$$d_L(z)_{th} = c(1+z)\int_0^z \frac{dz'}{H(z')} \tag{1.32}$$

Note that only from now and until the end of this subsection we will write the speed of light c explicitly.

We then define the dimensionless Hubble free luminosity distance:

$$D_L(z) = \frac{H_0 d_L}{c} \tag{1.33}$$

The apparent magnitude $m(z)_t h$ is related to D_L as:

$$m(z)_{th} = M + 5lg[D_L(z)] + 5lg[\frac{c/H_0}{Mpc}] + 25 \tag{1.34}$$

where the apparent magnitude m is defined as:

$$m = -2.5lg(\frac{l}{l_0}) \tag{1.35}$$

$lg(x) \equiv log_{10}(x)$, l is a reference flux, and the absolute magnitude M of a source is the apparent magnitude a source would have if it was 10pc away from earth. M is a calibration for the distance ladder approach (for example, geometric anchors - Cepheids - SNIa). By measuring the apparent magnitude we can determine $D_L(z)$ and subsequently H_0.

1.2.2 Solutions to the Hubble tension

As mentioned before, Hubble constant obtained through late-time and early-time methods is not consistent with each other and the results given by the former is usually larger. Here we review some of the attempts to alleviate the tension, for a list of solutions, see[15]

1. Void

The universe is not completely uniform, therefore, a possibility exists that we are living in an underdense region. If so, the local measurement of Hubble constant will be higher than the universal one, which can be observed from the following relation [16]:

$$\frac{\Delta H_0}{H_0} = -\frac{1}{3}\delta f(\Omega_m)\Theta(\delta, \Omega_m) \tag{1.36}$$

where δ is the local density contrast, $f(\Omega_m)$ is the growth rate of density perturbations and Θ is a non-linear correction which is small for typical size underdensities. From the above relation it is clear that underdensity, $\delta < 0$, leads to a higher local H_0. However, such a local void would cause large scale outflows, and it is found that the SNIa luminosity distance-redshift relation is not consistent with the local underdensity large enough to explain the Hubble tension at 4-5σ [17]. Along with other evidence (e.g.,[18]), this fact highly disfavours the void scenario.

2. Increasing N_{eff}

In ΛCDM, The energy density of radiation ρ_r is determined by photon energy density via the following relation:

$$\rho_r = \rho_\gamma[1 + \frac{7}{8}(\frac{4}{11})^{4/3} N_{eff}] \tag{1.37}$$

where N_{eff} is the number of relativistic degrees of freedom. To model the three neutrino species in Standard Model, we usually adopt $N_{eff} = 3.046$ [19]. An increase in N_{eff} means extra relativistic species and higher energy density at recombination, which leads to a higher H_0 according to the sound horizon - Hubble constant relation. However, as discussed in Section II.1, if we change ρ_r while fix ρ_b, peak heights in CMB spectra will be altered which conflicts with the current precise measurement. By allowing a self-interaction in the new species, it is possible for the peak heights to remain unchanged at the cost of change other cosmological parameters. Kreisch et al. [20] followed this idea and found $N_{edd} = 4.02 \pm 0.29$ as well as $H_0 = 72.3 \pm 1.4$. The problem with this scenario is that the self-interaction requires a mediator of mass keV - 100 MeV, which is subject to stringent cosmological and laboratory bounds [21].

3. Modified recombination

There exists other approaches to reduce the $r_s^\star$ without adding new components to the universe. Here we present some examples.

Varying electron mass. In [22] the recombination history is modified by assuming a time-dependent electron mass m_e. In order not to affect the CMB power spectra, the fractional variation Δ_x for quantity x, $x \in \omega_b, \omega_m, a_\star$ need to satisfy:

$$\Delta_{\omega_b} = \Delta_{\omega_m} = -\Delta_{a_\star} \tag{1.38}$$

where $a_\star$ is the scale factor at recombination and $\Delta_x \equiv log(x/x_{baseline})$. We also noticed that $r_s^\star \propto a_\star$. Through changing m_e we change the the energy levels of hydrogen E^H, which implies:

$$\Delta_{m_e} = -\Delta_{a_\star} \tag{1.39}$$

therefore, an increase in electron mass will lower $a_\star$, i,e. $r_s^\star$, making a varying m_e a possible solution to Hubble tension.

In order to resolve the tension, we need the electron mass at recombination to be about 5% larger than that at today. However, authors of [23] argue that increasing m_e at recombination will affect big bang nucleosynthesis (BBN): the helium fraction will become larger and the deuterium abundance will be smaller. Using BBN constraint, they conclude that m_e at BBN is only $\sim 1\%$ greater than its current value.

Similar modification to the recombination can also be achieved by increasing the fine structure constant α [22]: a stronger electromagnetic interaction means nuclei can star to form at higher temperature. That is, the recombination redshift $z_\star$ will increase which leads to a smaller $r_s^\star$. The problem with this modification is that, based on CMB power spectra, $\delta\alpha/\alpha$ is of order 10^{-3} [24]. The resulting change in the recombination sound horizon is too small to address the Hubble tension.

1.2.3 The EDE solution to the tension

Currently a promising approach to address the Hubble tension is early dark energy (EDE)(examples given below). EDE is a new component of the universe which is usually modeled as a scalar field. EDE is dynamically relevant at $z >> 1$ and its energy contribution is localized around recombination.

The addition of EDE can increase H_0 as follows. Again consider Eq (1.29), but this time a different $r_s^\star$ on the numerator due to EDE:

$$\theta_s^\star = \frac{H_0 r_s^{\star,ede}}{c\int_0^{z_\star}\frac{dz'}{E(z')}} \tag{1.40}$$

In Eq (1.27), $H(z') = (z', \rho_m, \rho_r)$ (again neglecting CC), and after introducing EDE, $H'(z') = (z', \rho_m, \rho_r, \rho_{ede})$. Apparently an extra component EDE will increase H(z) around recombination thus lower the comoving sound horizon, leading to an increase in H_0. In this sense EDE is expected to address the Hubble tension. This is supported by our analyses in Section III, where we show that the original $\sim 5\sigma$ tension is reduced to about 1.5σ. A plethora of EDE models have been proposed (for a review, see [9]). Here we give some examples of the models as well as briefly discuss some challenges to the EDE scenario.

- EDE models

Axion-like Early Dark Energy[25, 26]. In this model EDE is described by a canonical scalar field ϕ (i.e., its Lagrangian is X - V. X is the kinetic term) with $V(\theta) = m^2 f^2[1 - cos(\theta)]^n$, where m is the axion mass, f is the axion decay constant and $\theta = \phi/f$. This model is inspired by ultra-light axion and n=1 corresponds to the axion potential. It is a convention in

EDE models to use "phenomenological parameters", fractional EDE energy density f_{ede} and critical redshift z_c when doing analysis (detailed discussion can be found in the following section).

New Early Dark Energy (NEDE)[27, 28]. NEDE uses two scalar fields ψ and ϕ to model EDE, and has the following potential:

$$V(\psi,\phi) = \frac{\lambda}{4}\psi^4 + \frac{1}{2}\beta M^2\psi^2 - \frac{1}{3}\alpha M\psi^3 + \frac{1}{2}m^2\phi^2 + \frac{1}{2}\gamma\phi^2\psi^2. \tag{1.41}$$

where m, M is the mass of ϕ, ψ, respectively, $\lambda, \alpha, \beta, \gamma$ are dimensionless couplings. In NEDE a first-order phase transition occurs shortly before recombination. The energy density of DE after transition is lower than that before transition, and in this sense NEDE experience a decay around $z_\star$. NEDE model predicts a $H_0 = 71.4 \pm 1.0 km/s/Mpc$ and is compatible with SH0ES measurement they use (74.03 ± 1.42 km/s/Mpc) with $\sim 1.5\sigma$ difference.

Other EDE models includes EDE coupled to neutrinos [29] or DM [30][31], Acoustic Early Dark Energy (AEDE) [32], Rock 'n' Roll EDE [33], α-attractors EDE [34], Early Modified Gravity [35] in which the scalar field is coupled to the Ricci scalar, etc.

Challenges to EDE Though EDE provide possible solutions to Hubble tension, it introduces some new problems which need to be treated with care. One of these problems is the so-called second coincidence problem. In order to modify the sound horizon at recombination while keep the low-z universe unaffected, EDE must have a significant contribution to the total energy close to matter-radiation equality. It may be the case that there exists many EDE-like fields, but only the one active at matter-radiation equality catches our interest, because those become active latter behave just like DE while those become active at very early times can hardly affect the CMB [36][37][1806.10608]. However, one still needs to explain why there are so many such fields in the universe. Other problem includes:

S_8 tension: $S_8 \equiv \sigma_8(\Omega_m/0.3)^{0.5}$, where σ_8 is the the root-mean-squared of matter fluctuations on a $8h^{-1}$ Mpc scale. Weak lensing surveys (e.g., CFHTLenS [38]) give S_8 that is different from Planck's result at 2-3 σ. Unfortunately, the addition of EDE usually increases the inference of σ_8, leading to a greater tension. It is argued that the reason is EDE predicts higher CDM density.

No preference over EDE when excluding SH0ES: this a problem when analysing data using Markov Chain Monte Carlo (MCMC) analysis. When the dataset does not include a Gaussian prior on H_0 based on SH0ES measurement, usually it does not favor EDE over ΛCDM and predict a small value of f_{ede}. It is possibly caused by the prior volume effect which will be discussed in Section III.

1.3 Outline

The rest of this work is structured as follows: in Section II we will focus on the theory aspects of ξX^2 EDE model starting from its Lagrangian and using the least action principle to derive its EoM. Combining with Hubble equation equation and continuity equation for other components, it allows us to obtain a set of equations governing the background dynamics. The linear perturbation theory will also be discussed, before we move on to solve ξX^2 EDE's dynamics and study its properties in detail.

Section III is devoted to the Numeric Analysis of the model. We introduce our selection of cosmological datasets and model parameters for the MCMC analysis, which can be divided into ones with SH0ES and those without SH0ES. We find that these two choices give greatly different results in terms of reconstructed model parameters and best-fit χ^2, but all lead to the conclusion that ξX^2 EDE can reduce the Hubble tension. Changes to some other ΛCDM parameters are also discussed.

Finally, we give our conclusion and outlook in Section IV.

Chapter 2

Theory

2.1 From the principle of least action to equation of motion

We consider a general Lagrangian $\mathcal{L}$ for a field ϕ and the associated action:

$$\mathcal{S} = \int d^4x \sqrt{-g}\mathcal{L} \tag{2.1}$$

where $\mathcal{L} = \mathcal{L}(\phi, \triangledown_\mu \phi)$. If ϕ and $\triangledown_\mu \phi$ is changed by $\delta\phi$ and $\delta(\triangledown_\mu \phi) = \triangledown_\mu(\delta\phi)$, respectively, then:

$$\begin{aligned} \delta\mathcal{L} &= \mathcal{L}' - \mathcal{L} \\ &= \frac{\partial \mathcal{L}}{\partial \phi}\delta\phi + \frac{\partial \mathcal{L}}{\partial(\triangledown_\mu \phi)} \triangledown_\mu (\delta\phi) \end{aligned} \tag{2.2}$$

which leads to:

$$\delta\mathcal{S} = \int d^4x \sqrt{-g} \left[\frac{\partial \mathcal{L}}{\partial \phi}\delta\phi + \frac{\partial \mathcal{L}}{\partial(\triangledown_\mu \phi)} \triangledown_\mu (\delta\phi) \right] \tag{2.3}$$

integrating the second term on the right hand side by parts yields:

$$\begin{aligned} \sqrt{-g} \int d^4x \frac{\partial \mathcal{L}}{\partial(\triangledown_\mu \phi)} \triangledown_\mu (\delta\phi) = & \sqrt{-g} \int d^4x \triangledown_\mu \left(\frac{\partial \mathcal{L}}{\partial(\triangledown_\mu \phi)}\delta\phi\right) \\ & - \sqrt{-g} \int d^4x \triangledown_\mu \left(\frac{\partial \mathcal{L}}{\partial(\triangledown_\mu \phi)}\right)\delta\phi \end{aligned} \tag{2.4}$$

the first term can be converted to a surface term, therefore we can ignore it.

$$\therefore \delta\mathcal{S} = \sqrt{-g}\int d^4x\delta\phi\left[-\bigtriangledown_\mu(\frac{\partial\mathcal{L}}{\partial(\bigtriangledown_\mu\phi)}) + \frac{\partial\mathcal{L}}{\partial\phi}\right]$$

$$\delta\mathcal{S} = 0 \Rightarrow -\bigtriangledown_\mu(\frac{\partial\mathcal{L}}{\partial(\bigtriangledown_\mu\phi)}) + \frac{\partial\mathcal{L}}{\partial\phi} = 0 \tag{2.5}$$

which is the so-called Euler-Lagrange equation. Solving Eq (2.5) for a given $\mathcal{L}$ will result in its Equation of Motion (EoM).

2.2 ξX^2 EDE model

As mentioned before, EDE has mainly been studied with the canonical scalar field. In our model, we want to extend it to K-essence in which the kinetic term is generalized to $P(X)$. Explicitly, we consider a first order correction ξX^2. Adding a potential to drive the field evolution will result in the Lagrangian for the ξX^2 EDE model:

$$\mathcal{L} = X + \xi X^2 - V \tag{2.6}$$

where $X \equiv -\frac{1}{2}g^{\mu\nu}\bigtriangledown_\mu\phi\bigtriangledown_\nu\phi$, $V = V_0\phi^4$, $\xi, V_0 > 0$ are model parameters

Use E-L equation (2.5) and note that for a scalar field ϕ, $\bigtriangledown_\mu\phi$ is equivalent to $\partial_\mu\phi$, we have:

$$g^{\mu\nu}\bigtriangledown_\mu\bigtriangledown_\nu\phi - \xi\bigtriangledown_\mu(g^{\mu\nu}\partial_\nu\phi g^{\alpha\beta}\partial_\alpha\phi\partial_\beta\phi) - V_\phi = 0 \tag{2.7}$$

Expand Eq(2.7) and write down all terms explicitly:

$$\begin{aligned}\Rightarrow&\Box\phi - \xi[g^{\alpha\beta}\partial_\alpha\phi\partial_\beta\phi\Box\phi\\ &+ g^{\mu\nu}g^{\alpha\beta}\bigtriangledown_\mu(\partial_\alpha\phi)\partial_\nu\phi\partial_\beta\phi + g^{\mu\nu}g^{\alpha\beta}\bigtriangledown_\mu(\partial_\beta\phi)\partial_\nu\phi\partial_\alpha\phi] - V_\phi = 0\end{aligned} \tag{2.8}$$

where $\Box\phi \equiv g^{\mu\nu}\bigtriangledown_\mu\bigtriangledown_\nu\phi$, $V_\phi \equiv \frac{\partial V}{\partial\phi}$.

Eq (2.8) is the EOM of the scalar field ϕ in its most general form.

The energy-momentum tensor for a scalar field can be expressed as:

$$T_{\mu\nu} = -2\frac{1}{\sqrt{-g}}\frac{\delta(\sqrt{-g}\mathcal{L})}{\delta g^{\mu\nu}} \tag{2.9}$$

substitute into Lagrangian (2.6):

$$\delta(\sqrt{-g}\mathcal{L}) = \sqrt{-g}\left[-\frac{1}{2}\delta g^{\mu\nu}\partial\mu\phi\partial\nu\phi + \frac{\xi}{4}\delta g^{\mu\nu}g^{\alpha\beta}\partial_\mu\phi\partial_\nu\phi\partial_\alpha\phi\partial_\beta\phi\right.$$
$$\left.+\frac{\xi}{4}\delta g^{\alpha\beta}g^{\mu\nu}\partial_\mu\phi\partial_\nu\phi\partial_\alpha\phi\partial_\beta\phi\right] + \delta\sqrt{-g}\left[-\frac{1}{2}g^{\mu\nu}\partial_\mu\phi\partial_\nu\phi + \frac{\xi}{4}(g^{\mu\nu}\partial_\mu\phi\partial_\nu\phi)(g^{\alpha\beta}\partial_\alpha\phi\partial_\beta\phi) - V\right] \tag{2.10}$$

using

$$\frac{\delta\sqrt{-g}}{\delta g^{\mu\nu}} = -\frac{1}{2}\sqrt{-g}g_{\mu\nu}$$

and

$$\frac{\delta g^{\alpha\beta}}{\delta g^{\mu\nu}} = \frac{1}{2}(\delta^\alpha_\mu\delta^\beta_\nu + \delta^\alpha_\nu\delta^\beta_\mu)$$

It's straight forward to show that:

$$T_{\mu\nu} = \partial_\mu\phi\partial_\nu\phi - \xi g^{\alpha\beta}\partial_\mu\phi\partial_\nu\phi\partial_\alpha\phi\partial_\beta\phi - \frac{1}{2}g_{\mu\nu}g^{\alpha\beta}\partial_\alpha\phi\partial_\beta\phi$$
$$+ \frac{\xi}{4}(g^{\alpha\beta}\partial_\alpha\phi\partial_\beta\phi)(g^{\sigma\rho}\partial_\sigma\phi\partial_\rho\phi) - g_{\mu\nu}V \tag{2.11}$$

and

$$\begin{aligned} T^\mu_\nu &= g^{\mu\gamma}T_{\gamma\nu} \\ &= g^{\mu\gamma}\partial_\gamma\phi\partial_\nu\phi - \delta^\mu_\nu(\frac{1}{2}g^{\alpha\beta}\partial_\alpha\phi\partial_\beta\phi + V) - \xi g^{\alpha\beta}g^{\mu\gamma}\partial_\gamma\phi\partial_\nu\phi\partial_\alpha\phi\partial_\beta\phi \\ &+ \delta^\mu_\nu\frac{\xi}{4}(g^{\alpha\beta}\partial_\alpha\phi\partial_\beta\phi)(g^{\sigma\rho}\partial_\sigma\phi\partial_\rho\phi) \end{aligned} \tag{2.12}$$

We can use the energy-momentum tensor to calculate the energy density ρ_{ede} and pressure p_{ede} for the scalar field, i.e.:

$$\rho_{ede} = -T^0_0 \tag{2.13}$$
$$p_{ede} = \frac{1}{3}T^i_i \tag{2.14}$$

2.3 Background Dynamics of ξX^2 EDE

In the context of FLRW metric, Eq (2.8) simplifies to *:

$$\begin{aligned}&\frac{1}{a^2}(-\phi''-2\mathcal{H}\phi')-\xi[\frac{1}{a^4}(2\mathcal{H}\phi'^3+\phi''\phi'^2)\\&+g^{\mu\nu}g^{\alpha\beta}\bigtriangledown_\mu(\partial_\alpha\phi)\partial_\nu\phi\partial_\beta\phi+g^{\mu\nu}g^{\alpha\beta}\bigtriangledown_\mu(\partial_\beta\phi)\partial_\nu\phi\partial_\alpha\phi]-V_\phi=0\end{aligned}\tag{2.15}$$

To expand the remaining two (identical) terms in Eq (2.15), we use the fact that $\phi=\phi(t)$. It follows from the cosmological principle, i.e. isotropic and spatially homogeneous, so all background quantities are only function of time. Only $\mu=\nu=\alpha=\beta$ components will survive, which leads to:

$$\begin{aligned}&g^{\mu\nu}g^{\alpha\beta}\bigtriangledown_\mu(\partial_\alpha\phi)\partial_\nu\phi\partial_\beta\phi=g^{\mu\nu}g^{\alpha\beta}\bigtriangledown_\mu(\partial_\beta\phi)\partial_\nu\phi\partial_\alpha\phi\\&=^{\dagger}\frac{1}{a^4}\left[(\phi''-\mathcal{H}\phi)\phi'^2\right]\end{aligned}\tag{2.16}$$

Combining all terms gives:

$$(1+\frac{3\xi}{a^2}\phi'^2)\phi''+2\mathcal{H}\phi'+a^2V_\phi=0\tag{2.17}$$

which is the background EoM for scalar field ϕ.

Next, we calculate the energy density and pressure for the scalar field using results from the Section 2.2:

$$\Rightarrow\rho_{ede}=-T^0_0=\frac{1}{2}\frac{1}{a^2}\phi'^2+V+\frac{3\xi}{4}\frac{1}{a^4}\phi'^4=\frac{1}{2}\dot\phi^2+V+\frac{3\xi}{4}\dot\phi^4\tag{2.18}$$

$$p_{ede}=T^i_i=\frac{1}{2}\frac{1}{a^2}\phi'^2-V+\frac{\xi}{4}\frac{1}{a^4}\phi'^4=\frac{1}{2}\dot\phi^2-V+\frac{\xi}{4}\dot\phi^4\tag{2.19}$$

(no sum over i), where $\dot\phi\equiv\frac{d\phi}{dt}$

Rewriting Eq (2.17) in terms of $\dot\phi$,X and H instead of ϕ', ϕ'^2 and $\mathcal{H}$, we are able to give a set of equations governing the background dynamics of our model, after taking into account matter, radiation and cosmological constant:

*$\Box\phi=\frac{1}{a^2}(-\phi''-2\mathcal{H}\phi'),g^{\mu\nu}\partial_\mu\phi\partial_\nu\phi=-\frac{1}{a^2}\phi'^2,\mathcal{H}=\frac{a'}{a}$

$$
\begin{aligned}
H^2 = \frac{1}{3}(\rho_r + \rho_m + \rho_\Lambda + \rho_{ede}) &\equiv \frac{1}{3}\rho_{total} \\
\rho_{ede} &= \frac{1}{2}\dot{\phi}^2 + V + \frac{3\xi}{4}\dot{\phi}^4 \\
(1+6\xi X)\ddot{\phi} + 3H(1+2\xi X)\dot{\phi} + V_\phi &= 0 \\
\dot{\rho_m} &= -3H\rho_m \\
\dot{\rho_r} &= -4H\rho_r \\
\rho_\Lambda &= const.
\end{aligned} \tag{2.20}
$$

2.4 Linear perturbation

Here we consider linear perturbations to the field and the metric:

$$
\begin{aligned}
\phi^p(\eta, \mathbf{x}) &= \phi(\eta) + \delta\phi(\eta, \mathbf{x}) \\
g^p_{\mu\nu}(\eta, \mathbf{x}) &= g_{\mu\nu}(\eta) + \delta g_{\mu\nu}(\eta, \mathbf{x})
\end{aligned}
$$

where subscript p always denotes the perturbed quantities. In the following we omit the dependence of ϕ and $g_{\mu\nu}$ for simplicity.

In Newtonian gauge, the perturbed metric $g^p_{\mu\nu}$ is:

$$ds^2 = -a^2[(1+2\Psi)d\eta^2 - (1-2\Phi)d\mathbf{x}^2]$$

While

$$
\begin{aligned}
g^{00,p} &= -\frac{1}{a^2}\frac{1}{1+2\Psi} \approx -\frac{1}{a^2}(1-2\Psi) \\
g^{ii,p} &= \frac{1}{a^2}\frac{1}{1-2\Phi} \approx \frac{1}{a^2}(1+2\Phi)
\end{aligned}
$$

After perturbation, the first term in the EOM (2.8) becomes:

$$(\Box\phi)^p = g^{\mu\nu,p}[\partial_\mu\partial_\nu\phi^p - \Gamma^{\alpha,p}_{\mu\nu}\partial_\alpha\phi^p] \tag{2.21}$$

after expansion

$$(\Box\phi)^p = -\frac{1}{a^2}[\phi'' + 2\mathcal{H}\phi' - (\Psi' + 3\Phi' + 4\mathcal{H}\Psi)\phi' - 2\mathcal{H}\phi'' + \delta\phi'' + 2\mathcal{H}\delta\phi' - \nabla^2\delta\phi] \tag{2.22}$$

The second term in the EOM (2.8) is more involved:

$$
\begin{aligned}
&(-\xi[g^{\alpha\beta}\partial_\alpha\phi\partial_\beta\phi\Box\phi + g^{\mu\nu}g^{\alpha\beta}\bigtriangledown_\mu(\partial_\alpha\phi)\partial_\nu\phi\partial_\beta\phi + g^{\mu\nu}g^{\alpha\beta}\bigtriangledown_\mu(\partial_\beta\phi)\partial_\nu\phi\partial_\alpha\phi])^p \\
=& -\xi[g^{\alpha\beta,p}\partial_\alpha\phi^p\partial_\beta\phi^p\cdot(\Box\phi)^p && \langle A\rangle \\
&+ g^{\mu\nu,p}g^{\alpha\beta,p}(\partial_\mu\partial_\alpha\phi^p - \Gamma^{\rho,p}_{\mu\alpha}\partial_\rho\phi^p)\partial_\nu\phi^p\partial_\beta\phi^p && \langle B\rangle \\
&+ g^{\mu\nu,p}g^{\alpha\beta,p}(\partial_\mu\partial_\beta\phi^p - \Gamma^{\rho,p}_{\mu\beta}\partial_\rho\phi^p)\partial_\nu\phi^p\partial_\alpha\phi^p && \langle C\rangle]
\end{aligned} \tag{2.23}
$$

all components in $\langle B\rangle$ and $\langle C\rangle$ except for $\mu = \nu = \alpha = \beta = 0$ are of second or higher order or equal 0. Therefore,

$$
\begin{aligned}
&\langle B\rangle = \langle C\rangle \\
&= g^{00,p}g^{00,p}(\phi'' + \delta\phi'' - \Gamma^{\rho,p}_{00}\partial_\rho\phi^p)(\phi' + \delta\phi')^2 \\
&\approx \frac{1}{a^4}[(\phi')^2\phi'' - \mathcal{H}(\phi')^3 - 4\Psi(\phi')^2\phi'' + (-\Psi' + 4\mathcal{H}\Psi)(\phi')^3 + (\phi')^2\delta\phi'' + (2\phi'\phi'' - H(\phi')^2)
\end{aligned} \tag{2.24}
$$

we now have:

$$
\begin{aligned}
(2.23) = -\frac{\xi}{a^4}[&3(\phi')^2\phi'' - 12\Psi(\phi')^2\phi'' - 3(\Psi' + \Phi')(\phi')^3 \\
&+ 3(\phi')^2\delta\phi'' + 6\phi'\phi''\delta\phi' - (\phi')^2\nabla^2\delta\phi]
\end{aligned} \tag{2.25}
$$

Finally, the third term in the EOM (2.8) simply become:

$$
(-V_\phi)^p = -V_\phi - V_{\phi\phi}\delta\phi \tag{2.26}
$$

Instead of working in real space where $\delta\phi = \delta\phi(\eta, \mathbf{x})$, we can do a Fourier transform and go to the k-space:

$$
\delta\phi_k(\eta, \mathbf{k}) = \int \frac{1}{(2\pi)^{\frac{3}{2}}}\delta\phi(\eta, \mathbf{x})e^{i\mathbf{k}\cdot\mathbf{x}}d\mathbf{x}
$$

where in k-space $\delta\phi(\eta, \mathbf{x})$ is replaced by $\delta\phi_k(\eta, \mathbf{k})$. The benefits of going to k-space is that linear perturbation equations decouple into independent equations for each Fourier mode. The dependence on spatial coordinates vanishes and the evolution for each Fourier mode $\delta\phi_k(\eta, \mathbf{k})$ only depends on its time derivative and $k = |\mathbf{k}|$.

After Fourier transform, the EOM for $\delta\phi_k$ is:

$$
\begin{aligned}
&[1 + \frac{3\xi}{a^2}(\phi')^2]\delta\phi_k'' + [2\mathcal{H} + \frac{6\xi}{a^2}\phi'\phi'']\delta\phi_k' + [k^2 + a^2V_{\phi\phi} + \frac{\xi}{a^2}(\phi')^2k^2]\delta\phi_k = \\
&[2\Psi + \frac{12\xi}{a^2}\Psi(\phi')^2]\phi'' + [\Psi' + 3\Phi' + 4\mathcal{H}\Psi + \frac{3\xi}{a^2}(\Psi' + \Phi')(\phi')^2]\phi'
\end{aligned} \tag{2.27}
$$

The energy density perturbation and pressure perturbation, $\delta\rho_{ede}$ and δp_{ede}, for the scalar field can be obtained:

$$\delta\rho_{ede} = (\dot{\phi} + 3\xi\dot{\phi}^3)\delta\dot{\phi} + V_\phi \delta\phi \tag{2.28}$$

$$\delta p_{ede} = (\dot{\phi} + \xi\dot{\phi}^3)\delta\dot{\phi} - V_\phi \delta\phi \tag{2.29}$$

Similarly, we can also obtain the heat flux of the scalar fluid:

$$\begin{aligned} (\rho_{ede} + p_{ede})\theta &\equiv ik^j \delta T^0_j \\ (\rho_{ede} + p_{ede})\sigma &\equiv -(\hat{k}_i \cdot \hat{k}_j - \frac{1}{3}\delta_{ij})\Sigma^i_j \\ \Sigma^i_j &\equiv T^i_j - \delta^i_j T^k_k/3 \end{aligned} \tag{2.30}$$

The linearized Einstein equation yields [39]

$$\begin{aligned} -k^2\Phi + 3\mathcal{H}(-\dot{\Phi} + \mathcal{H}\Psi) &= -4\pi G a^2 \delta\rho_{ede} \\ k^2(-\dot{\Phi} + \mathcal{H}\Psi) &= 4\pi G a^2 (\rho_{ede} + p_{ede})\theta \\ -\ddot{\Phi} + \mathcal{H}(\dot{\Psi} - 2\dot{\Phi}) + (2\frac{\ddot{a}}{a} - \mathcal{H}^2)\Psi - \frac{k^2}{3}(\Phi + \Psi) &= \frac{4\pi}{3} G a^2 \delta p_{ede} \\ -k^2(\Phi + \Psi) &= 12\pi G a^2 (\rho_{ede} + p_{ede})\sigma \end{aligned} \tag{2.31}$$

which, supplemented with the evolution equations of ordinary species, see [39], and Eq (2.27 - 2.30) equation, form a close system describing the linear perturbation dynamics.

2.5 Evolution of the field

We explore the background dynamics by implementing the closed system of equations Eq (2.20) in Mathematica. To simplify the calculation we use x $\equiv$ log(a) as the time variable.

We give our results in Figure (2.1 - 2.3). Figure (2.1) can roughly illustrate the behaviour of the field: Initially the field is frozen at some non-zero ϕ_i. Its energy density is subdominant and remains nearly constant like a cosmological constant. As the Hubble parameter decreases over time, at some redshift the Hubble energy scale becomes roughly of the same order of magnitude as the effective mass of the scalar field, i.e.:

$$H^2 \sim V_{\phi\phi} \tag{2.32}$$

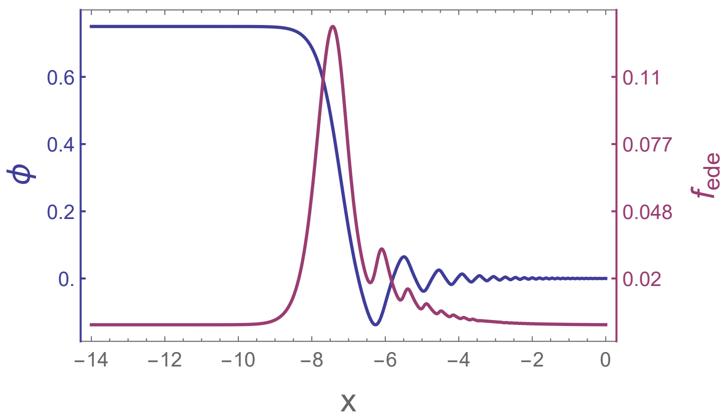

(a) $V_0 = 10^{10}, \phi_i = 0.75, \xi = 10^{-11}$

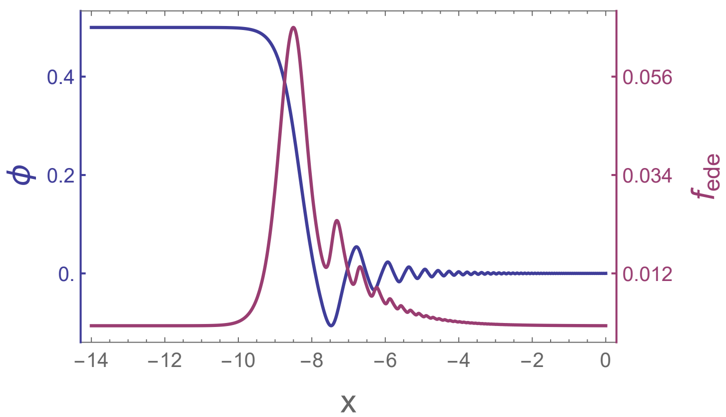

(b) $V_0 = 10^{12}, \phi_i = 0.5, \xi = 10^{-12}$

Figure 2.1: *Evolution of ϕ and f_{ede} for two sets of initial conditions. EDE with these initial conditions can produce the desired observables.*

At this stage its energy fraction $f_{ede}(z)$ increases with time because the energy density of the dominant species (radiation) redshifts with time. $f_{ede}(z)$ peaks at a critical redshift z_c when the field starts to roll (i.e., when Eq (2.32) is satisfied[‡]) and quickly drops afterwards due to Hubble damping when the field experiences damped oscillation around its potential minimum. $f_{ede}(z_c)$ is hereinafter refereed to as f_{ede}.

We also present in Figure (2.2a) the evolution of equation of the state parameter for the EDE $w_{ede}(x)$ as well as the effective equation of the state parameter for the universe $w_{eff}(x)$, where $w_{eff}(x) = p_{total}/\rho_{total}$, p_{total}

[‡]The field unfreezes when the driving force (proportional to the mass of the field at this moment) is comparable to the damping ($\sim H^2$)

is the overall pressure of all components in the Universe. In these examples we use model parameters $\{\phi_i, V_0, \xi V_i\} = \{0.5, 10^{12}, 1\}$. We use $\xi V_i \equiv \xi V_0 \phi_i^4$ instead of ξ because, as we will explain in detail later in this section, it is the parameter that is directly relevant to the non-canonical dynamical behavior of the field. This set of parameters roughly corresponds to the best-fit values of $\{f_{ede}, z_c, \xi V_i\}$ we get in the MCMC analysis, thus being representative. The evolution of energy density ρ_i for each component of the Universe is also given in Figure (2.2b), where i can represent matter, radiation, CC and EDE. We can conclude that at early time the Universe is radiation-dominated and gradually evolves towards a matter-dominated era, before it finally experience accelerated expansion caused by both CC and EDE. Although $w_{ede}(x)$ oscillates rapidly at low redshift, we can tell from figure (2.2b)) that in average it decays with $w \sim \frac{1}{3}$ (which may vary slightly depending on the three model parameters), i.e., the scalar field studied mimics radiation at late times.

However, the dynamics of the field may change dramatically if we change some of the model parameters. Figure (2.3a - 2.3c) shows the consequences of increasing ϕ_i, V_0, and ξ, respectively. In all three cases the Universe evolution becomes dominated by the scalar field, which drastically changes the evolution of the field. We note that this is not realistic.

As we observe from Fig (2.1) and (2.3), when some of the three model parameters V_0, ξ and ϕ_i become too large, the EDE will not experience a physically acceptable evolution. This motivates us to look for more physically intuitive parameters, instead of ϕ_i, V_0 and ξ, to parameterize the model. From previous literature, (as concluded in [9]), a good set of parameters is $\{f_{ede}, z_c\}$, where f_{ede} is the maximal energy fraction of the scalar field and z_c is the critical redshift when the energy fraction reaches this maximum, as explained before. One needs one parameter in place of ξ

To this end we notice that the Lagrangian for the EDE Eq (2.6) can be written as:

$$\mathcal{L} = X(1 + \xi X) - V$$

where ξX, hereinafter refereed to as the kinetic correction, measures the degree to which the non-canonical kinetic term deviates from the canonical kinetic term X. ξX is a function of time $\xi X = \xi X(z)$ that has a maximum value $(\xi X)_{max}$ at some redshift z_m around z_c (see Figure (2.4), again we use parameters $\{\phi_i, V_0, \xi V_i\} = \{0.5, 10^{12}, 1\}$). $(\xi X)_{max}$, or simply X_{max} since ξ is a number in our model, is a perfect choice for the fourth parameter. However, $(\xi X)_{max}$ is not a combination of V_0, ξ and ϕ_i itself, so we find a quantity, ξV_i, that has a close relation with $(\xi X)_{max}$. Eq (2.17) is an oscillation equation and when there is no damping, one has $V_{max} = X_{max}$, where V_{max} is the maximal potential energy. In case of the EDE, because of damping, the first oscillation has most energy, thus both V_{max} and X_{max} appears in the first oscillation. For the first oscillation, V_i determines V_{max}, thus also determines X_{max}. We expect this to be a linear relation, and verifies this guess in the following.

For a given $(\xi X)_{max}$ and ϕ_i, we can find a ξ for each V_0 such that the field with initial condition ϕ_i, V_0, ξ has that $(\xi X)_{max}$. Figure 2.5 shows ξ versus V_0 for four different ϕ_i. We observe that ξV_i is roughly the same for all ϕ_i, i.e., ξV_i does not depend on ϕ_i, so the next is fixing ϕ_i and calculate ξV_i for different $(\xi X)_{max}$. We find that there is a linear relationship between them (as shown in Figure 2.6), which supports our conjecture.

Most of EDE models, as concluded in [9], has a $z_c \in [10^3, 10^4]$ and a $f_e de$ around 0.1. We adopt [9]'s range of z_c and allow $f_e de$ to take values up to 0.5. As shown in Figure (2.7), within our interested range, for each ξV_i, we can always find some $\{\phi_i, V_0\}$ that correspond to a certain $\{f_{ede}, z_c\}$. It is achieved via the so-called shooting procedure introduced in Sec. 3.1.

ϕ_i largely controls the value of f_{ede}, while V_0 largely controls the value of z_c. Note that as ξV_i increases, f_{ede} grows faster with ϕ_i, while the growth of z_c become slower when increasing V_0.

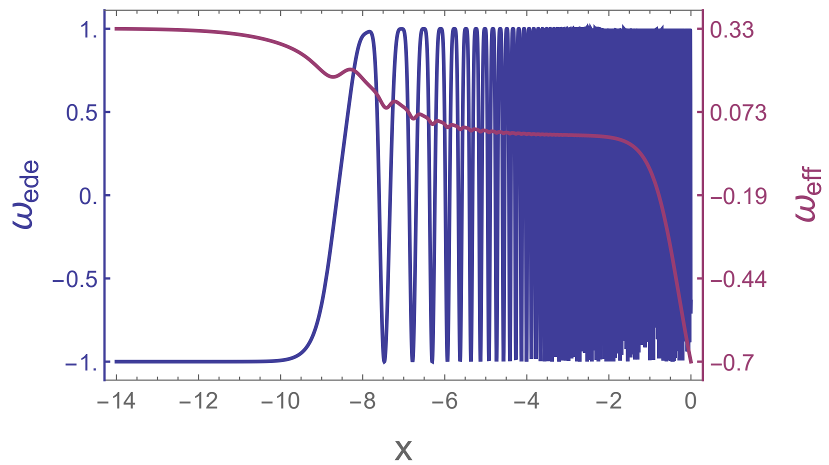

(a) *$\omega_{eff} - x$ (red) and $\omega_{ede} - x$ (blue)*

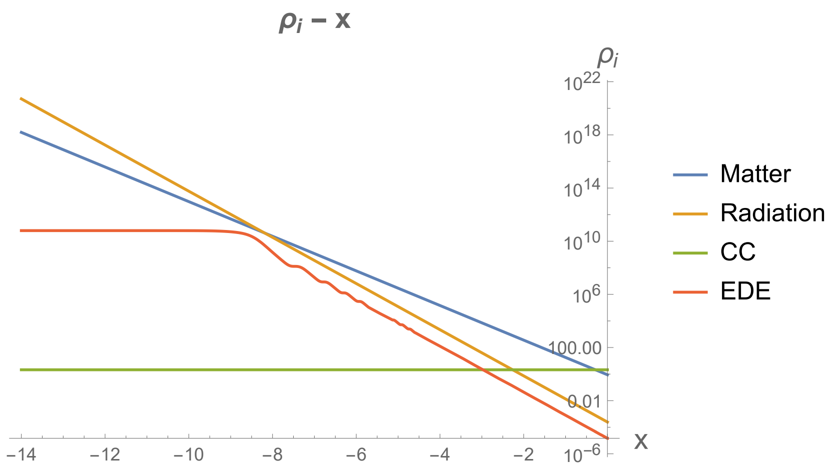

(b) *$\rho_i - x, i \in \{matter, radiation, CC, EDE\}$*

Figure 2.2: *Evolution of ω_{eff}, ω_{ede} and different components' energy density*

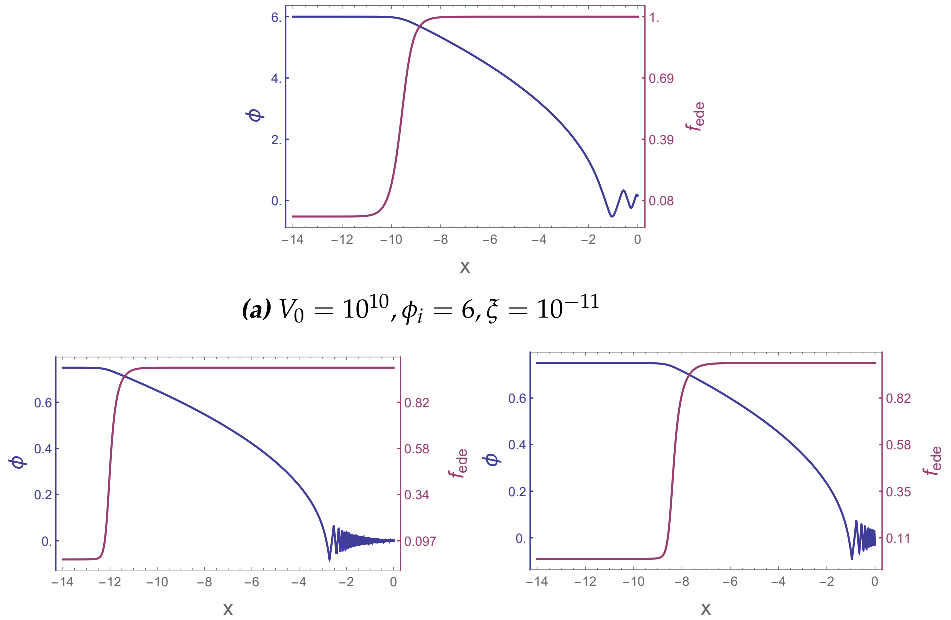

(a) $V_0 = 10^{10}, \phi_i = 6, \xi = 10^{-11}$

(b) $V_0 = 10^{16}, \phi_i = 0.75, \xi = 10^{-11}$ ***(c)*** $V_0 = 10^{10}, \phi_i = 0.75, \xi = 5 \times 10^{-6}$

Figure 2.3: *Evolution of ϕ and f_{ede} for three sets of initial conditions. These represents unhealthy behaviours of the scalar field*

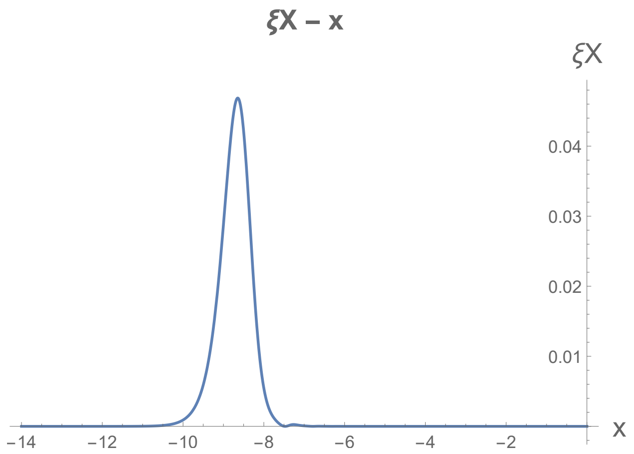

Figure 2.4: *Kinetic correction as a function of x,* $\{\phi_i, V_0, \xi V_i\} = \{0.5, 10^{12}, 1\}$

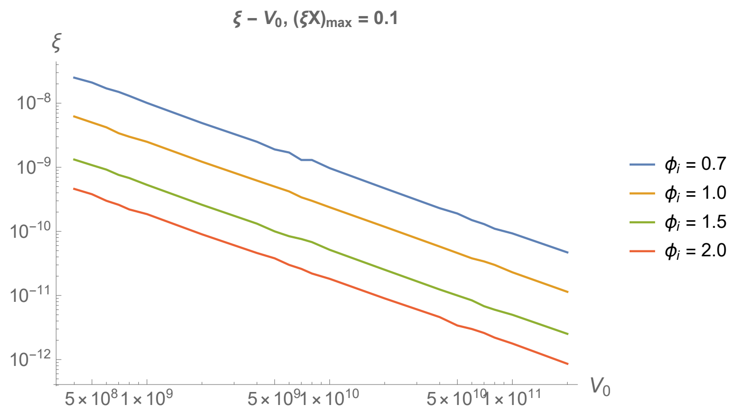

Figure 2.5: *ξ as a function of V_0, fixing $(\xi X)_{max}$ and varying ϕ_i*

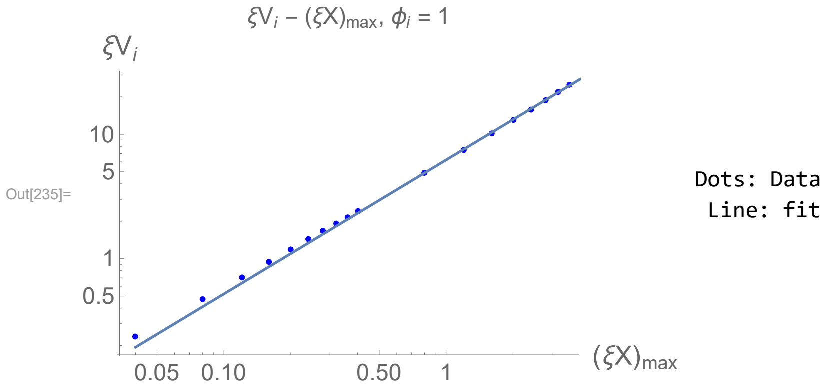

Figure 2.6: *ξV_i as a function of $(\xi X)_{max}$, fixing ϕ_i*

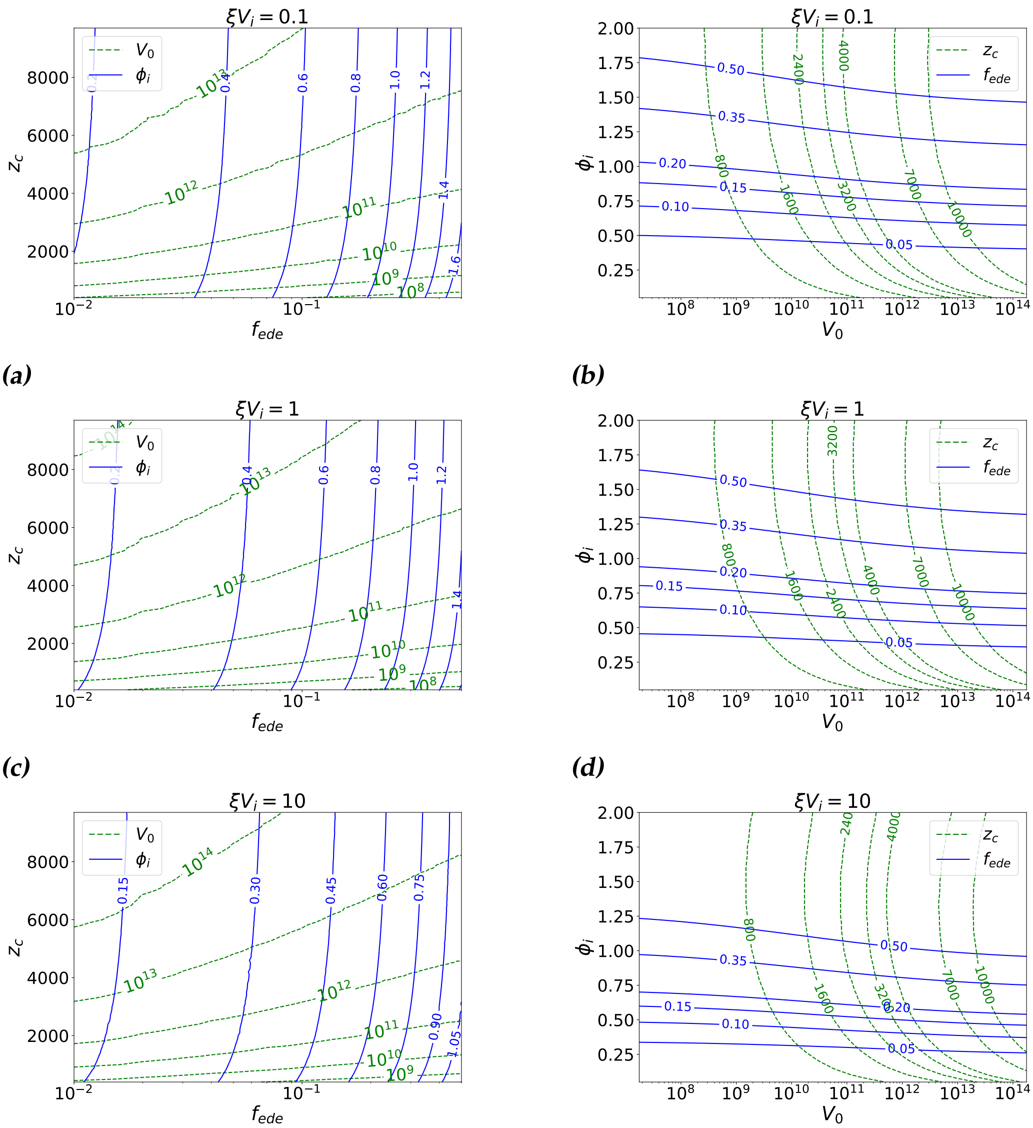

(a) *(b)* *(c)* *(d)* *(e)* *(f)*

Figure 2.7: *Contours, first and second column: contours for ϕ_i, V_0 and z_c, f_{ede}, respectively. Three rows: fixing $\xi Vi = 0.1, 1, 10, fromtomtobottom$.*

Chapter 3

Numeric Analysis

3.1 Analysis Methods

We run MCMC chains using the public code COBAYA [40][41]. We perform the analysis with a Metropolis-Hasting algorithm. When analysing ξX^2 EDE model, we assume flat priors on:

$$\{\Omega_b h^2, \Omega_c h^2, H_0, n_s, log(10^{10}A_s), \tau_{reio}, f_{ede}, log(1+z_c), lg(\xi V_i)\}$$

. As for standard ΛCDM model, we assume flat priors on:

$$\{\Omega_b h^2, \Omega_c h^2, H_0, n_s, log(10^{10}A_s), \tau_{reio}\}$$

where $h = H_0/(100km/s/Mpc)$ is today's value of the dimensionless Hubble parameter, $n_s$is the primordial scalar spectral index, A_s is the initial super-horizon amplitude of curvature perturbations and τ_{reio} is the reionization optical depth. For each model, we run two MCMC chains with and without SH0ES prior on H_0 [10]. Details of each parameter's prior can be found at Table (3.1).

We use a modified version of EFTCAMB [42][43][44][45] to solve background equations and implement a shooting method to calculate model parameters ($\{\phi_i, V_0\}$ using physical quantities $\{f_{ede}, z_c\}$). This is achieved as follows:

Given $\{f_{ede,i}, z_{c,i}\}$, we want to find the corresponding $\{\phi_i, V_0\}$. However, camb can only do the inverse process, performing a map M: M($\{\phi_i, V_0\}$) = $\{f_{ede}, z_c\}$. The standard method is then to use the scipy.optimize.root function in python to find the root for the equation:

$$
\begin{aligned}
f_{ede,x}/f_{ede,i} - 1 &= 0 \\
z_{c,x}/z_{c,i} - 1 &= 0
\end{aligned}
\tag{3.1}
$$

where $M(\{\phi_{i,x}, V_{0,x}\}) = \{f_{ede,x}, z_{c,x}\}$ and $\{\phi_{i,x}, V_{0,x}\}$ is the initial condition we want to derive. In order to speed up the root function, a proper initial guess of $\{\phi_{i,x}, V_{0,x}\}$ is needed. We used the following guess:

$$
\begin{aligned}
V_0 &\sim \frac{\rho_{fid}}{16 f_{ede}} \\
\phi_i &\sim 2\sqrt{f_{ede}}
\end{aligned}
\tag{3.2}
$$

where ρ_{fid} is the fiducial energy density of the universe assuming negligible CC and EDE energy. It we assume that EDE's kinetic energy is small compared to its potential until z_c, we can get the following approximate relations:

$$
\begin{aligned}
V(\phi_i) &= 3H_c^2 f_{ede} \\
V_{\phi\phi} &= 9H_c^2
\end{aligned}
\tag{3.3}
$$

where $3H_c^2 = 3H(z_c)^2 = \rho_{fid}(z_c)$. The second line in Eq (3.3) implies that the scalar field's initial mass (also its mass at z_c under our assumption) is proportional to the Hubble mass at z_c. Solving the above equations we can have Eq (3.2).

We adopt Planck's assumption [11] on neutrino and model them as two massless species and a single massive species with mass $m_\nu = 0.06eV$.

The following consists of our datasets:

- **Planck NPIPE (PR4) CamSpec high-ℓ TTTEEE** [46]
- **Planck 2018 low-ℓ TT and EE** [11]
- **Planck 2018 lensing** [11]
- **SH0ES' measurement of H_0 [10]:** $H_0 = 73.04 \pm 1.04 kms^{-1}Mpc^{-1}$
- **The Pantheon dataset [47]**, which measures the luminosity distance of 1048 Type-Ia supernovae ranging from redshift $0.01 < z < 2.3$
- **BAO datasets:** the BAO 6dFGS at redshift z = 0.106 [48], BAO SDSS DR7 at redshift z = 0.15 [49], and BAO SDSS DR16 [50].

Parameter	Prior
$\Omega_b h^2$	$0.01 < \Omega_b h^2 < 0.03$
$\Omega_c h^2$	$0.1 < \Omega_c h^2 < 0.15$
H_0 (km/s/Mpc)	$60 < H_0 < 80$
n_s	$0.8 < n_s < 1.2$
$log(10^{10} A_s)$	$1.61 < log(10^{10} A_s) < 3.91$
τ_{reio}	$0.01 < \tau_{reio} < 0.8$
f_{ede}	$0 < f_{ede} < 0.3$
$log(1 + z_c)$	$7 < log(1 + z_c) < 10$
$lg(\xi V_i)$	$-2 < lg(\xi V_i) < 5$

Table 3.1: *Priors for model parameters used in MCMC*

We choose the above datasets under these considerations: for an EDE model, Planck's measurement of CMB is necessary since it constraints the physics around last-scattering, which is exactly the time when EDE manifests itself, lowering the sound horizon and lifting the Hubble constant; BAO is closely related to CMB and measures the physics of another time period; luminosity distance of supernovae places a tight constraint on the late-time revolution of the universe, while SH0ES' measurement of H_0 is the most contributing part of the tension.

Convergence of an MCMC run is assessed using the Gelman-Rubin criterion R-1 < 0.05.

We report the reconstructed mean(best fit) value of the cosmological parameters, as well as their 1σ confidence interval in Table 3.2 (with SH0ES) and Table 3.3 (without SH0ES), while the best-fit χ^2 for each experiment and each dataset are given in Table 3.4 (with SH0ES) and Table 3.5(without SH0ES). In Figure (3.1) and (3.2), we plot the reconstructed posterior distributions for both models.

Parameter	ΛCDM with SH0ES	EDE with SH0ES
H_0	$68.27(68.49)^{+0.45}_{-0.47}$	$71.09(71.42)^{+0.84}_{-0.72}$
$100\Omega_b h^2$	$2.239(2.246)^{+0.012}_{-0.015}$	$2.245(2.237)^{+0.021}_{-0.020}$
$\Omega_c h^2$	$0.1175(0.1172)^{+0.0009}_{-0.0010}$	$0.1285(0.1289)^{+0.0037}_{-0.0031}$
n_s	$0.9690(0.9702)^{+0.0043}_{-0.0041}$	$0.9815(0.9851)^{+0.0060}_{-0.0047}$
$log(10^{10}A_s)$	$3.051(3.054)^{+0.014}_{-0.015}$	$3.063(3.064) \pm 0.014$
τ_{reio}	$0.061(0.063)^{+0.007}_{-0.008}$	$0.058(0.059)^{+0.006}_{-0.007}$
f_{ede}	-	$0.086(0.091)^{+0.022}_{-0.019}$
$log(1+z_c)$	-	$8.195(8.254)^{+0.162}_{-0.207}$
$lg(\xi V_i)$	-	$-0.169(0.183)^{+0.563}_{-0.314}$

Table 3.2: *The mean(best fit) value and $\pm 1\sigma$ error for cosmological parameters reconstructed from the MCMC analysis with SH0ES.*

Parameter	ΛCDM w/o SH0ES	EDE w/o SH0ES
H_0	$67.51(67.37)^{+0.50}_{-0.38}$	$68.60(68.01)^{+0.64}_{-0.91}$
$100\Omega_b h^2$	$2.225(2.221)^{+0.012}_{-0.013}$	$2.223(2.205)^{+0.015}_{-0.017}$
$\Omega_c h^2$	$0.1192(0.1194)^{+0.0008}_{-0.0012}$	$0.1219(0.1195)^{+0.0013}_{-0.0030}$
n_s	$0.9651(0.9641)^{+0.0038}_{-0.0037}$	$0.9697(0.9702)^{+0.0047}_{-0.0057}$
$log(10^{10}A_s)$	$3.044(3.040)^{+0.012}_{-0.015}$	$3.048(3.046)^{+0.014}_{-0.015}$
τ_{reio}	$0.056(0.054)^{+0.006}_{-0.008}$	$0.057(0.055)^{+0.006}_{-0.007}$
f_{ede}	-	$0.029(0.007)^{+0.007}_{-0.029}$
$log(1+z_c)$	-	$8.694(9.948)^{+0.775}_{-0.835}$
$lg(\xi V_i)$	-	$-0.321(1.213)^{+1.038}_{-0.799}$

Table 3.3: *The mean(best fit) value and $\pm 1\sigma$ error for cosmological parameters reconstructed from the MCMC analysis without SH0ES.*

Datasets	ΛCDM with SH0ES	EDE with SH0ES
Planck high-ℓ TTTEEE	10550.40	10549.90
Planck low-ℓ TT,EE	420.86	417.75
Planck lensing	9.40	9.73
BAO	23.55	22.51
Pantheon	1034.77	1034.74
SH0ES	19.15	2.43
Total χ^2_{min}	12058.20	12037.00
$\Delta\chi^2_{min}$	0	-21.20

Table 3.4: *The best fit χ^2 per dataset for ΛCDM and EDE with SH0ES. For comparison, a Λ CDM fit to $Planck$ only yields $\chi^2_{high-\ell}$ = 10545.4, $\chi^2_{low-\ell}$ = 419.14 and $\chi^2_{lensing}$ = 9.04*

Datasets	ΛCDM w/o SH0ES	EDE w/o SH0ES
Planck high-ℓ TTTEEE	10543.90	10542.10
Planck low-ℓ TT,EE	419.24	418.15
Planck lensing	8.93	9.25
BAO	24.78	23.03
Pantheon	1035.16	1035.06
Total χ^2_{min}	12032.00	12027.60
$\Delta\chi^2_{min}$	0	-4.4

Table 3.5: *The best fit χ^2 per dataset for ΛCDM and EDE, without SH0ES*

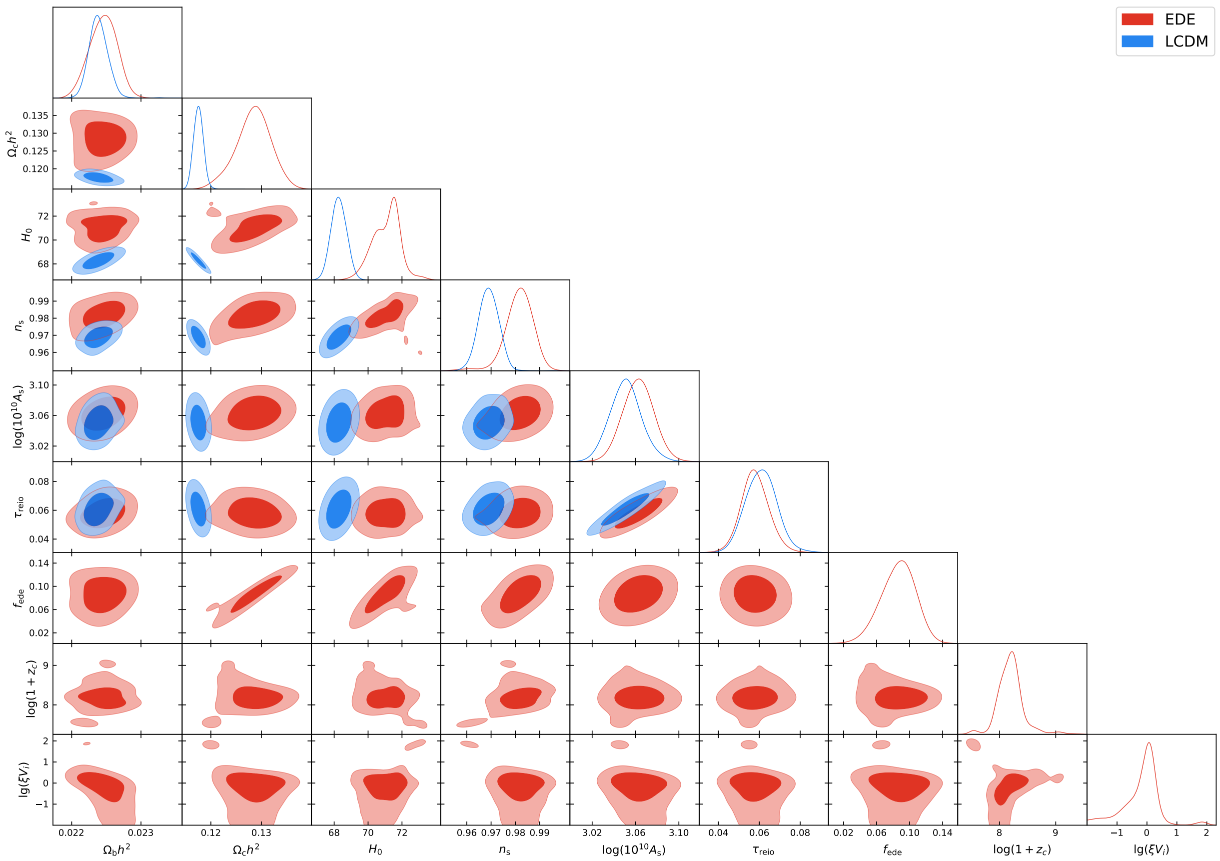

Figure 3.1: *Marginalized 1D and 2D posterior distributions of cosmological parameters, with SH0ES. Red: EDE, Blue: ΛCDM*

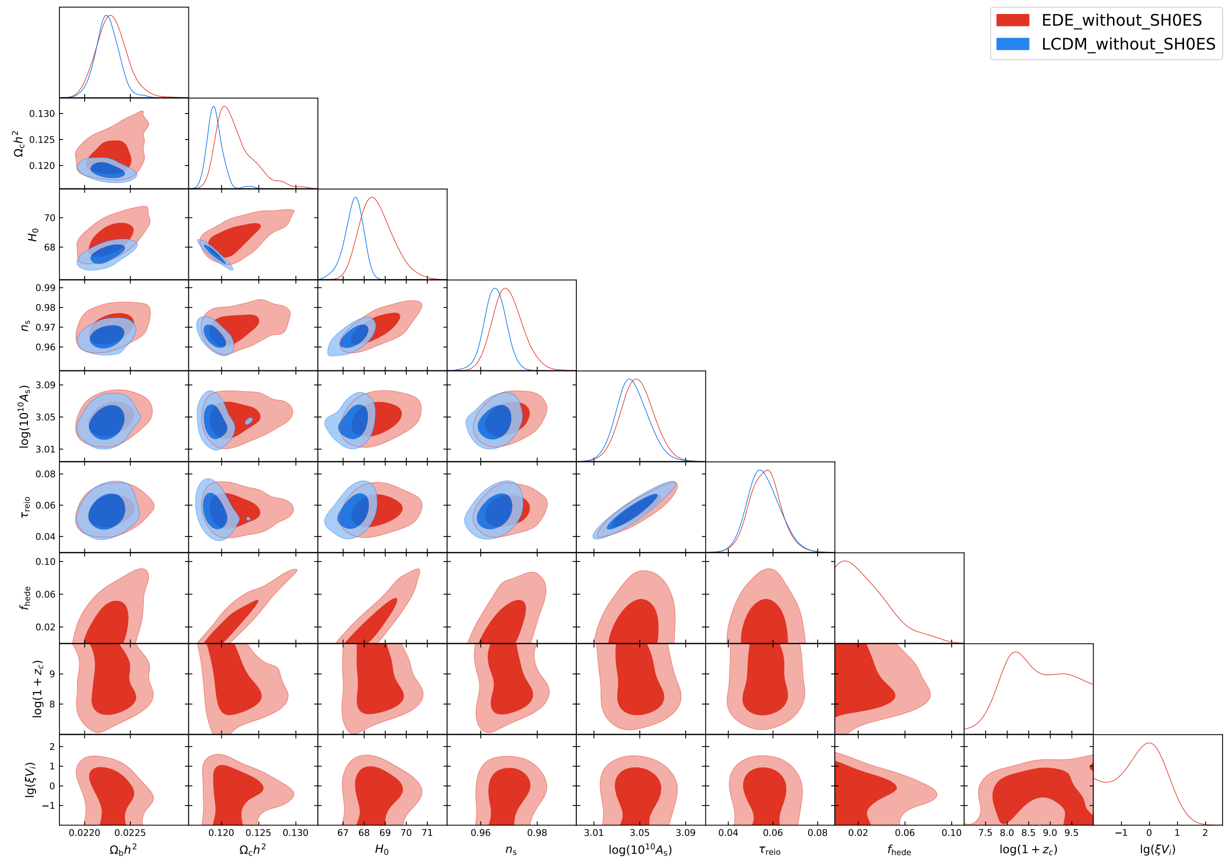

Figure 3.2: *Marginalized 1D and 2D posterior distributions of cosmological parameters, without SH0ES. Red: EDE, Blue: ΛCDM*

3.2 Implications of the reconstructed parameters

Table 3.3 shows the reconstructed parameters obtained in MCMC analysis without including SH0ES measurement of H_0. Before discussing the six ΛCDM parameters, let us begin with the three EDE parameters f_{ede}, $log(1+z_c)$ and ξV_i.

At the first sight these parameters appears abnormal: the EDE's maximal energy budget, f_{ede} has a relatively small mean value (0.029) and a negligible best-fit value (0.007), along with a highly-asymmetrical $\pm 1\sigma$ interval, which essentially means the existence of EDE is strictly constrained by the datasets. $log(1+z_c)$ and ξV_i's best-fit value is extremely large, lying around their 2σ limit. We can also observe from Fig(3.2) that the contours for the above parameters is high non-Gaussian.

[9] argues that this is caused by the so-called 'prior volume effects'. Due to the nature of EDE model, only f_{ede} is correlated with H_0 (recall that f_{ede} serves to reduce the sound horizon at recombination, thus leading to a higher H_0), while $log(1+z_c)$ and ξV_i is not defined when $f_{ede} \to 0$. If the datasets do not favour a non-zero f_{ede} (that is, when SH0ES prior is absent), the remaining two parameters will have no effect on the data, leading to increased ΛCDM - like volume and a strong upper limits on EDE.

Because of the prior volume effects, analysis without SH0ES is unlikely to provide us with insights into the EDE model. In the rest of this subsection, we will discuss the results we obtained via MCMC analysis with the SH0ES prior.

As shown in Table 1, the ξX^2 model shares the general characteristics of the EDE models, namely that its maximal fractional energy contribution to the total energy is $\sim$ 10% (about 9% in our case) at a critical redshift before recombination. The left model parameter, ξV_i, has a best-fit value about 1.52.

The ξX^2 EDE predicts a $100\omega_b = 2.239(2.246)^{+0.012}_{-0.015}$, which is consistent with ΛCDM value with only 0.25 σ difference. It is a unique feature of ξX^2 EDE which worth some discussion.

In the previous papers about EDE, the authors usually report that EDE gives a higher ω_b, (denoted as $\omega_{b,ede}$) compared with ΛCDM's value $\omega_{b,\Lambda CDM}$. For example, in [33] $\omega_{b,ede}$ is about 1 σ higher than $\omega_{b,\Lambda CDM}$ (n=2 case), in [28] the difference is $\sim$ 1.5σ (with SH0ES). Other two papers, [51] and [31] also report differences of about 1.3 and 1.4 σ, respectively. In fact, this common increase in ω_b and the cause is first reported in [52], which argues that the fractional change in ω_b with respect to ΛCDM is proportional to the fractional change in D_A:

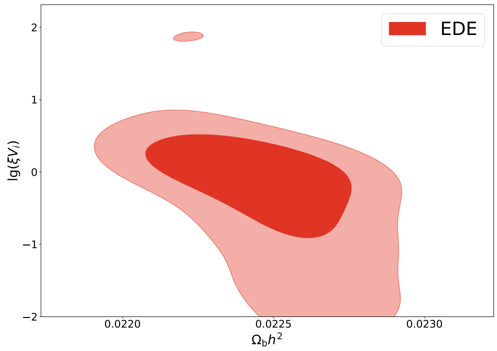

Figure 3.3: *Contour for ω_b and ξV_i in ξX^2 EDE model*

$$\frac{\delta\omega_b}{\omega_b} \sim -(1-\alpha)\frac{\delta D_A}{D_A}$$

where D_A is the angular diameter distance to the last-scattering surface and $0 < \alpha < 1$ is a parameter representing the inaccuracy of high-ℓ CMB data.

The consistency between $\omega_{b,ede}$ and $\omega_{b,\Lambda CDM}$ in ξX^2 EDE model means that there exists a degeneracy between ω_b and ξV_i. As we can observe in Fig (3.3), as ξV_i increases, ω_b is forced to have lower value, i.e., we trades a non-zero ξV_i for an unchanged ω_b. This reveals one of the interesting effects of adding a ξX^2 term to the canonical kinetic term X.

In our EDE model, ω_c increased dramatically by $\sim 3.1\ \sigma$. [52] predicts the change in ω_c to be:

$$\frac{\delta\omega_c}{\omega_c} \sim 2\frac{\delta H_0}{H_0} \tag{3.4}$$

eq (3.4) yields $\delta\omega_c \sim 0.0073$, which is a good approximation for our result.

Due to a larger ω_c and an unchanged ω_b, ξX^2 EDE model gives an increased ω_m, this is indeed the consequence of varying H_0 while keeping today's CMB temperature fixed. [53] argues that, based on CMB and BAO constraints, ω_m and h_0 obeys the following relation:

$$\omega_m^{-1} h_0^2 \simeq const.$$

thus a higher H_0 (consequently h_0) leads to a higher ω_m.

The primordial spectral index n_s is $\sim 1.7\ \sigma$ larger in EDE, while the initial super-horizon amplitude of curvature perturbations A_s in EDE is consistent with that in ΛCDM with $\sim 0.6\ \sigma$. In our MCMC run, ΛCDM gives a $n_s \sim 7\ \sigma$ away from 1, while [11] gives $\sim 9\ \sigma$. EDE lowers this value to $\sim 3\ \sigma$, which shows EDE's potential to challenge the well-known paradigm of slow-roll inflation [52]. The change in A_s have influence on the physics of CMB lensing, but we will leave it for further exploration. Finally, we observe that the reionization optical depth τ_{reio} is almost the same in EDE and ΛCDM with a minor 0.3 σ's discrepancy.

The most significant change occurs in today's Hubble parameter H_0, which strongly favour the ξX^2 EDE model over ΛCDM. To make a comparison, ΛCDM' H_0 (68.27) is in tension with SH0ES' measurement with 4.2 σ's difference, while the EDE prediction is compatible with SH0ES' measurement with $\sim 1.5\sigma$ difference. This illustrates ξX^2 EDE model's ability to address the Hubble tension. We note that, on the one hand, the ξX^2 EDE model behaves better than most of the models (not only EDE models) reviewed in [54] (Also note that the authors of [54] concludes that EDE is a favoured kind of models). On the other hand, among a collection of eight kind of EDE models[9], only two models, NEDE and axion-like EDE, does better, reducing Hubble tension to $\sim 1.2\sigma$ and $\sim 1.1\sigma$, respectively. However, we must say this is not a rigours statement since different models use different datasets and analysis methods (for example, they use different prior on H_0, depending on which SH0ES release they choose). Despite this concern, the above reasoning still shows that EDE is one of the most likely solution to the Hubble tension, and among various kind of EDE models our ξX^2 EDE model deserves scientific interests.

3.3 χ^2 Analysis

Following what we did in the previous section, we begin by discussing the best-fit χ^2 for experiments without SH0ES prior (Table 3.5). The best-fit χ^2 is reduced by -4.4 compared with ΛCDM. Improvements come from the fit to *Planck* high-ℓ (-1.80), *Planck* low-ℓ (-1.09) and BAO (-1.75), while the fit to *Planck* lensing is worsened (by +0.32). EDE behaves as good as ΛCDM when fitting the Pantheon Super Novae Ia dataset.

It might seem like that EDE is not strongly favoured since χ^2 is only reduced by 4.4. However, this is again due to the prior volume effects. Though we cannot find from Table 3.5 evidence for EDE, we can use another metric Q_{DMAP} measuring the level of tension, suggested in [54][55], to support the EDE:

$$Q_{DMAP} = \sqrt{\chi^2(with\,SH0ES) - \chi^2(w/o\,SH0ES)} \tag{3.5}$$

(in units of Gaussian σ). Such metric can better capture the effects of non-Gaussianity in the posterior distribution, which is the case of Fig (3.2). Combining with information in Table 3.4, we have:

$$Q_{\Lambda CDM} \sim 5.1\sigma, Q_{EDE} \sim 3.1\sigma$$

which tells us EDE helps resolve the Hubble tension.

Next we move forward to the experiments done with SH0ES prior, whose results are given in Table 3.4. We find in Table 3.4 that the best-fit χ^2 is reduced by -21.2 compared with ΛCDM (greatly larger compared with Table 3.5). The major improvement comes from SH0ES value of H_0, contributing ~ -16.7 to χ^2_{min}. We note that the addition of the EDE does not spoil the fit to Planck dataset, in contrast, the best-fit χ^2 is improved by -3.3. For comparison, we also give in Table 3.4 the results for a fit to *Planck* only. The fit to BAO is also improved by ~ 1 while we don't find a statistically significant difference between the two model's fit with respect to Pantheon dataset.

We observe from the above discussion that, no matter comparing the best-fit ξ^2 or using the metric Q, the datasets favour EDE over ΛCDM.

Chapter 4

Conclusion and Outlook

There has been a increasing tension between Hubble constant measured in local regions using luminosity distance - redshift relation and those inferred from CMB and BAO under the assumption of ΛCDM, recently reaching $\sim 5\sigma$ level. It is proved that this discrepancy is not liked to be caused by simple explanations, e.g., measurement uncertainty (for reviews, see[56],[57]) or a large void around the earth. In addition, SNIa data place tight bound on the deviation to late-time expansion history, thus strongly constraints the late-time modifications to ΛCDM [58][59][60]. Under this situation, changing the physics in the early-time become a favoured approach which can, e.g., decrease the sound horizon at recombination to increase the inferred H_0. Among these solutions, EDE does well in maintaining good fit to CMB spectra as well as in reducing the tension to a low level. Unlike many previous EDE models that assuming a canonical scalar field, we consider introducing a first-order correction to the canonical kinetic term, namely ξX^2, which is inspired by K-essence DE[7].

In Section II, starting from the least action principle and the proposed Lagrangian of ξX^2 EDE and in the context of FLRW metric, we derived EDE's background as well as linearly perturbed EoM. When combined with Hubble equation, background energy density of EDE and continuity equation for matter, radiation and CC, we obtain a group of closed equations that governs the background dynamics. We then focused on the evolution of the EDE scalar field. Generally speaking, in ξX^2 EDE the scalar field is frozen at its initial value at early times behaving as CC before it starts to roll, quickly drop and finally oscillates around its potential minimum. From Figure (2.2b) we are able to read EDE's dilution rate and find it dilutes like radiation at late times. The entire history of EoS parameter for the whole universe w_{eff} is depicted in Figure (2.2a) which exhibits three stages of radiation, matter and CC domination, successively.

Apart from the commonly used phenomenological parameters, the energy fraction of EDE f_{ede} and critical redshift z_c, we introduce the third physically meaningful parameter ξVi to replace the original ξ, as it has a linear relation with the maximum value of kinetic correction ξX. Using shooting method, we give plots for constant V_0, ϕ_i as well as z_c, f_{ede} in Figure (2.7). Roughly speaking, V_0, ϕ_i determines the value of f_{ede} and z_c, respectively.

In Section III, we presented our numerical results. We run MCMC chains using a combination of the following datasets: Planck NPIPE (PR4) CamSpec high-ℓ TTTEEE, Planck 2018 low-ℓ TT and EE, Planck 2018 lensing, Pantheon, BAO datasets as well as a SH0ES prior on H_0 (MCMC without SH0ES are also performed for comparison). We use flat priors on (some function of) the six ΛCDM parameter as well as the three phenomenological parameters for ξX^2 EDE model. Reconstructed mean (best-fit) value and $\pm 1\sigma$ interval as well as best-fit χ^2 for each dataset are reported in Table 2-5, while the posterior distribution is given in Fig (3.1) and (3.2).

Table 3 and 5 are results for MCMC analysis without SH0ES. Judging from them alone it seems that EDE not favoured by the data, since mean and best-fit value for f_{ede} is small. However, it is caused by the prior volume effect. If we use a different metric called Q_{DAMP} which compares the difference between best-fit χ^2 analysed with and without SH0ES, we are able to find that ξX^2 EDE is favoured over ΛCDM. Table 2 and 4 are for analysis with SH0ES prior which is more resourceful. First, values of f_{ede} and z_c hints at an EDE that has a non-negligible ($\sim 10\%$) contribution to the total energy before recombination. The ξVi is 2σ non-zero which supports the existence of the non-canonical kinetic term. As expected, the most significant improvement compared with ΛCDM happens in H_0, reducing the Hubble tension to only $\sim 1.5\sigma$. As for ω_c and n_s, the value predicted by EDE is about 3.1 and 1.7 σ larger, respectively, while the value for τ_{reio} and A_s is consistent with ΛCDM with $\sigma < 1$. It is surprising to find ω_b in EDE is compatible with ΛCDM with only $\sim 0.25\ \sigma$ difference, which is at odds with many previous models where a $> 1\sigma$ discrepancy is found. It points at an interesting effect of the non-canonical kinetics term and shows that we can trade a non-zero ξV_i for an unchanged ω_b. While reducing the Hubble tension, the ξX^2 EDE does not spoil the fit to dataset, improving it by -21.2. In addition, the fit to Planck datasets alone is improved by -3.3, showing EDE's advantage over ΛCDM.

Some details of ξX^2 EDE need to be further investigated. In future works, we hope to gain a better understanding of the effect of non-canonical kinetic term, for example, explaining the reason for an unchanged ω_b after introducing EDE. It is also appealing to investigate other possible form of non-canonical correction, as now we are using the simple first-order connection ξX^2. Finally, we can Use more detailed statistical methods (e.g., profile likelihood, Bayes evidence) to quantify tension in ξX^2 EDE model.

Chapter 5

Acknowledgements

I would like to express my gratitude to Alessandra. Your expertise in the field of cosmology as well as friendliness help me a lot at the beginning of the project. Also thanks for being supportive during my research and providing with many useful advice.

My thanks to Subodh for helping me with the paper works as the second supervisor; My thanks to Gen for the daily support. You are always ready for my question and willing to help me with all aspects of the project even with minor issues. Finally I would like thank my parents and friends. Your caring for me is of great importance.

Chapter 6

References

[1] Riess, Adam G., et al. ”Observational evidence from supernovae for an accelerating universe and a cosmological constant.” The astronomical journal 116.3 (1998): 1009.

[2] Carroll, Sean M., William H. Press, and Edwin L. Turner. ”The cosmological constant.” In: Annual review of astronomy and astrophysics. Vol. 30 (A93-25826 09-90), p. 499-542. 30 (1992): 499-542.

[3] Padmanabhan, Thanu. ”Gravity and the thermodynamics of horizons.” Physics Reports 406.2 (2005): 49-125.

[4] Padmanabhan, Thanu. ”Cosmological constant-the weight of the vacuum.” Physics reports 380.5-6 (2003): 235-320.

[5] Wetterich, Christof. ”Cosmology and the fate of dilatation symmetry.” Nuclear Physics B 302.4 (1988): 668-696.

[6] Zlatev, Ivaylo, Limin Wang, and Paul J. Steinhardt. ”Quintessence, cosmic coincidence, and the cosmological constant.” Physical Review Letters 82.5 (1999): 896.

[7] Armendariz-Picon, Christian, V. Mukhanov, and Paul J. Steinhardt. ”Essentials of k-essence.” Physical Review D 63.10 (2001): 103510.

[8] Chow, Nathan, and Justin Khoury. ”Galileon cosmology.” Physical Review D-Particles, Fields, Gravitation, and Cosmology 80.2 (2009): 024037.

[9] Poulin, Vivian, Tristan L. Smith, and Tanvi Karwal. ”The Ups and Downs of Early Dark Energy solutions to the Hubble tension: a review of models, hints and constraints circa 2023.” Physics of the Dark Universe (2023): 101348.

[10] Riess, Adam G., et al. ”A comprehensive measurement of the local value of the Hubble constant with 1 km s- 1 Mpc- 1 uncertainty from the Hubble Space Telescope and the SH0ES team.” The Astrophysical journal letters 934.1 (2022): L7.

[11] Aghanim, Nabila, et al. ”Planck 2018 results-VI. Cosmological parameters.” Astronomy & Astrophysics 641 (2020): A6.

[12] Efstathiou, George, and J. Richard Bond. ”Cosmic confusion: degeneracies among cosmological parameters derived from measurements of microwave background anisotropies.” Monthly Notices of the Royal Astronomical Society 304.1 (1999): 75-97.

[13] Komatsu, Eiichiro, et al. ”Five-year wilkinson microwave anisotropy probe* observations: cosmological interpretation.” The Astrophysical Journal Supplement Series 180.2 (2009): 330.

[14] Hu, Wayne, and Martin White. ”Measuring the curvature of the universe.” arXiv preprint astro-ph/9606140 (1996).

[15] Hu, Jian-Ping, and Fa-Yin Wang. ”Hubble tension: The evidence of new physics.” Universe 9.2 (2023): 94.

[16] Huterer, Dragan. ”Growth of cosmic structure.” The Astronomy and Astrophysics Review 31.1 (2023): 2.

[17] Kenworthy, WD’Arcy, Dan Scolnic, and Adam Riess. ”The local perspective on the Hubble tension: local structure does not impact measurement of the Hubble constant.” The Astrophysical Journal 875.2 (2019): 145.

[18] Wu, Hao-Yi, and Dragan Huterer. ”Sample variance in the local measurements of the Hubble constant.” Monthly Notices of the Royal Astronomical Society 471.4 (2017): 4946-4955.

[19] Mangano, Gianpiero, et al. ″Relic neutrino decoupling including flavour oscillations.″ Nuclear Physics B 729.1-2 (2005): 221-234.

[20] Kreisch, Christina D., Francis-Yan Cyr-Racine, and Olivier Doré. ″Neutrino puzzle: Anomalies, interactions, and cosmological tensions.″ Physical Review D 101.12 (2020): 123505.

[21] Blinov, Nikita, et al. ″Constraining the self-interacting neutrino interpretation of the Hubble tension.″ Physical Review Letters 123.19 (2019): 191102.

[22] Sekiguchi, Toyokazu, and Tomo Takahashi. ″Early recombination as a solution to the H_0 tension.″ Physical Review D 103.8 (2021): 083507.

[23] Seto, Osamu, and Yo Toda. ″Big bang nucleosynthesis constraints on varying electron mass solution to the Hubble tension.″ Physical Review D 107.8 (2023): 083512.

[24] Hart, Luke, and Jens Chluba. ″New constraints on time-dependent variations of fundamental constants using Planck data.″ Monthly Notices of the Royal Astronomical Society 474.2 (2018): 1850-1861.

[25] Poulin, Vivian, et al. ″Early dark energy can resolve the Hubble tension.″ Physical review letters 122.22 (2019): 221301.

[26] Smith, Tristan L., Vivian Poulin, and Mustafa A. Amin. ″Oscillating scalar fields and the Hubble tension: a resolution with novel signatures.″ Physical Review D 101.6 (2020): 063523.

[27] Niedermann, Florian, and Martin S. Sloth. ″New early dark energy.″ Physical Review D 103.4 (2021): L041303.

[28] Niedermann, Florian, and Martin S. Sloth. ″Resolving the Hubble tension with new early dark energy.″ Physical Review D 102.6 (2020): 063527.

[29] Sakstein, Jeremy, and Mark Trodden. ″Early dark energy from massive neutrinos as a natural resolution of the Hubble tension.″ Physical review letters 124.16 (2020): 161301.

[30] Karwal, Tanvi, et al. ″Chameleon early dark energy and the Hub-

ble tension." Physical Review D 105.6 (2022): 063535.

[31] McDonough, Evan, et al. "Early dark sector, the Hubble tension, and the swampland." Physical Review D 106.4 (2022): 043525.

[32] Lin, Meng-Xiang, et al. "Acoustic dark energy: Potential conversion of the Hubble tension." Physical Review D 100.6 (2019): 063542.

[33] Agrawal, Prateek, et al. "Rock 'n'roll solutions to the Hubble tension." Physics of the Dark Universe 42 (2023): 101347.

[34] Braglia, Matteo, et al. "Unified framework for early dark energy from α-attractors." Physical Review D 102.8 (2020): 083513.

[35] Braglia, Matteo, et al. "Early modified gravity in light of the H 0 tension and LSS data." Physical Review D 103.4 (2021): 043528.

[36] Arvanitaki, Asimina, et al. "String axiverse." Physical Review D-Particles, Fields, Gravitation, and Cosmology 81.12 (2010): 123530.

[37] Karwal, Tanvi, and Marc Kamionkowski. "Early dark energy, the Hubble-parameter tension, and the string axiverse." arXiv preprint arXiv:1608.01309 (2016).

[38] Heymans, Catherine, et al. "CFHTLenS: the Canada-France-Hawaii telescope lensing survey." Monthly Notices of the Royal Astronomical Society 427.1 (2012): 146-166.

[39] Ma, Chung-Pei, and Edmund Bertschinger. "Cosmological perturbation theory in the synchronous and conformal Newtonian gauges." arXiv preprint astro-ph/9506072 (1995).

[40] Torrado, Jesus, and Antony Lewis. "Cobaya: Code for Bayesian Analysis of hierarchical physical models." Journal of Cosmology and Astroparticle Physics 2021.05 (2021): 057.

[41] https://ascl.net/1910.019

[42] Lewis, Antony, Anthony Challinor, and Anthony Lasenby. "Efficient computation of cosmic microwave background anisotropies in closed Friedmann-Robertson-Walker models." The Astrophysical Journal 538.2

(2000): 473.

[43] Lewis, Antony, and Sarah Bridle. "Cosmological parameters from CMB and other data: A Monte Carlo approach." Physical Review D 66.10 (2002): 103511.

[44] Hu, Bin, et al. "Effective field theory of cosmic acceleration: an implementation in CAMB." Physical Review D 89.10 (2014): 103530.

[45] Raveri, Marco, et al. "Effective Field Theory of Cosmic Acceleration: constraining dark energy with CMB data." Physical Review D 90.4 (2014): 043513.

[46] Rosenberg, Erik, Steven Gratton, and George Efstathiou. "CMB power spectra and cosmological parameters from Planck PR4 with CamSpec." Monthly Notices of the Royal Astronomical Society 517.3 (2022): 4620-4636.

[47] Scolnic, Daniel Moshe, et al. "The complete light-curve sample of spectroscopically confirmed SNe Ia from Pan-STARRS1 and cosmological constraints from the combined pantheon sample." The Astrophysical Journal 859.2 (2018): 101.

[48] Beutler, Florian, et al. "The 6dF Galaxy Survey: baryon acoustic oscillations and the local Hubble constant." Monthly Notices of the Royal Astronomical Society 416.4 (2011): 3017-3032.

[49] Ross, Ashley J., et al. "The clustering of the SDSS DR7 main Galaxy sample-I. A 4 per cent distance measure at z= 0.15." Monthly Notices of the Royal Astronomical Society 449.1 (2015): 835-847.

[50] Alam, Shadab, et al. "Completed SDSS-IV extended Baryon Oscillation Spectroscopic Survey: Cosmological implications from two decades of spectroscopic surveys at the Apache Point Observatory." Physical Review D 103.8 (2021): 083533.

[51] Berghaus, Kim V., and Tanvi Karwal. "Thermal friction as a solution to the Hubble and large-scale structure tensions." Physical Review D 107.10 (2023): 103515.

[52] Ye, Gen, Bin Hu, and Yun-Song Piao. "Implication of the Hubble

tension for the primordial Universe in light of recent cosmological data." Physical Review D 104.6 (2021): 063510.

[53] Ye, Gen, and Yun-Song Piao. "T 0 censorship of early dark energy and AdS vacua." Physical Review D 102.8 (2020): 083523.

[54] SchÃ¶neberg, Nils, et al. "The H0 Olympics: A fair ranking of proposed models." Physics Reports 984 (2022): 1-55.

[55] Raveri, Marco, and Wayne Hu. "Concordance and discordance in cosmology." Physical Review D 99.4 (2019): 043506.

[56] Abdalla, Elcio, et al. "Cosmology intertwined: A review of the particle physics, astrophysics, and cosmology associated with the cosmological tensions and anomalies." Journal of High Energy Astrophysics 34 (2022): 49-211.

[57] Di Valentino, Eleonora, et al. "In the realm of the Hubble tension-a review of solutions." Classical and Quantum Gravity 38.15 (2021): 153001.

[58] Bernal, Jose Luis, Licia Verde, and Adam G. Riess. "The trouble with H0." Journal of Cosmology and Astroparticle Physics 2016.10 (2016): 019.

[59] Poulin, Vivian, et al. "Implications of an extended dark energy cosmology with massive neutrinos for cosmological tensions." Physical Review D 97.12 (2018): 123504.

[60] Aylor, Kevin, et al. "Sounds discordant: Classical distance ladder and ΛCDM-based determinations of the cosmological sound horizon." The Astrophysical Journal 874.1 (2019): 4.

[61] Perivolaropoulos, Leandros, and Foteini Skara. "Challenges for ΛCDM: An update." New Astronomy Reviews 95 (2022): 101659.
2105.05208